SUPPLEMENTARY METHODS

Cell culture and treatment

Human primary keratinocytes were isolated from the foreskins of ten patients who underwent urological surgery, as previously described. Keratinocytes were maintained in complete media (EpiLife, Thermo Fisher, USA) supplemented with 60 μM calcium and EpiLife Defined Growth Supplement. HaCaT cells were cultured in Dulbecco's modified Eagle's medium (DMEM) supplemented with fetal bovine serum (FBS; NEST Biotechnology) at 37 °C in a 5% carbon dioxide incubator. For the SJS/TEN cell model, keratinocytes were treated with 50 μg/mL LL-37 and 50 ng/mL Ac2-26 for 30 h, unless indicated otherwise. Cell line was authenticated by STR profiling within 6 months of the study.

Cell viability assays and necrosis analysis

The keratinocytes were seeded into 96-well plates at a density of 5000 cells per well. Following treatment, 10 μl of CCK-8 reagent (Beyotime, Shanghai, China) was added. The absorbance of each well was detected at a wavelength of 450 nm by a multimode plate reader. Cellular necrosis was evaluated by Annexin V/propidium iodide (PI) double-staining assay by flow cytometry (BD Biosciences).

Intracellular ROS detection

The keratinocytes were incubated with 10 μM DCFH-DA for 30 min in the dark at 37 °C. The intracellular ROS concentration was measured using a fluorescence microplate reader (Thermo Fisher Scientific).

Adenosine triphosphate (ATP) measurement

ATP levels were determined with an ATP assay kit (Thermo Fisher Scientific) according to the manufacturer's instructions.

Lactate dehydrogenase (LDH) release assay

Cytotoxicity was assessed using a LDH assay kit (Beyotime, Shanghai, China) following the manufacturer's instructions. Absorbance was measured at 490 nm using a microplate reader (SYNERGY H4, BioTek, USA).

Expression vector construction and transient transfection

Small interfering RNAs (siRNAs) against *OGT* were purchased from Huzhou Hippobiotec Co., Ltd., and transfected at a final concentration of 100 nM using Lipofectamine RNAiMAX (Thermo Fisher) according to the manufacturer's protocol. The plasmid containing the OGT cDNA was synthesized by Huzhou Hippobiotec Co., Ltd. The sequences are listed in Table 3.

Electron microscopy

The keratinocytes were immediately fixed at 4 °C with 2% glutaraldehyde in 0.1 M sodium cacodylate buffer, postfixed for 1 h on ice with 1% osmium tetroxide, rinsed with distilled water, dehydrated in acetonitrile and graded methanol (50%, 20 min; 70%, 20 min; 95%, 20 min; and 100%, 20 min), embedded in epoxy resin (EMbed-812; USA) and polymerized at 70 °C overnight. The thin sections were cut and stained with lead citrate and uranyl acetate, followed by imaging with a Hitachi H600 electron microscope (Hitachi, Japan).

Western blotting

Cells were lysed in denaturing cell extraction buffer. The lysates were resolved by SDS–PAGE and transferred to PVDF membranes (Bio-Rad). The membranes were blocked with 5% nonfat milk and probed with primary antibodies (Table 4). HRP-conjugated goat secondary antibodies were incubated with the membrane at room temperature for 1 h (Table 4). The signals were detected using HyGLO chemiluminescence reagent (Denville Scientific) on a Bio-Rad ECL system.

Total RNA extraction and quantitative real-time PCR

Total RNA was extracted using TRIzol reagent (Invitrogen, 15596018). cDNA was obtained using the AMV reverse transcription system (Takara, 2621). Quantitative real-time PCR was performed with SYBR Green PCR premix reagent (ABI, 4472908) and specific primers (Table 5).

Immunohistochemical (IHC) staining

The tissue sections were incubated with 3% H_2O_2 for 15 min to eliminate endogenous peroxidase activity, subjected to antigen retrieval in a microwave, and incubated with primary antibodies overnight at 4 °C. After washes with PBST, the sections were incubated with the appropriate secondary antibodies for 1 h at room

temperature. Antigen–antibody complexes were detected using DAB substrate (Gene Tech, Shanghai, China).

Generation of OGT-knockout HaCaT cell lines

Guide RNA sequences for CRISPR/Cas9 were designed using the CRISPR design website (http://crispr.mit.edu/). The oligonucleotide sequence for human OGT gRNA #1 was 5'-CACCGTTGGCACATCGAGAATATC-3'/ 5'-AAACGATATTCTCGATGTGCCAAC-3'. The OGT gRNAs targets exon 2 of the OGT gene. Complementary gRNA oligonucleotides were annealed and cloned and inserted into the pHBLV-U6-gRNA-EF1-CRISPR/Cas9-Puro vector (Hanbio Biotechnology Co. Ltd., Shanghai, China). HaCaT cells were transfected with pHBLV-U6/gRNA #1 using Lipofiter^{TM} according to the manufacturer's instructions. Two days after transfection, the cells were treated with puromycin for three days. Colonies were isolated after two weeks, and OGT gene editing was verified by DNA sequencing and Western blotting.

TUNEL (Terminal dexynucleotidyl transferase (TdT)-mediated dUTP nick end labeling) staining

The tissue sections were dewaxed and rehydrated as above described. Then, the slides were digested with Proteinase K at 55 °C for 1 h and stained using a TUNEL apoptosis kit (Gugeshengwu, Wuhan, China) according to manufacturer's instructions. An Olympus BX51 system was used to observe TUNEL-positive cells.

Co-immunoprecipitation

The cell lysates were incubated with the primary antibody for 2 h at 4 °C, after which 20 μL of resuspended Protein A/G Plus-Agarose (sc-2003, Santa Cruz) was added. After an overnight rotation at 4 °C, the beads were centrifuged at 1000 × g for 5 min at 4 °C, washed with PBS, resuspended in 40 μL of sample buffer, and boiled for 10 minutes to elute the proteins. The eluted proteins were analyzed by western blotting.

Enzyme-linked immunosorbent assay (ELISA)

The concentrations of RIPK1, RIPK3, IL-6, IL-1β and TNF-α in serum and cell supernatant were assayed using RIPK1 (Cell Signaling Technology, Cat#40446),

RIPK3 (Abcam, Cat#ab209384 and Cell Signaling Technology, Cat#74771), IL-6 (Abcam, Cat#ab178013 and Cat#ab222503), IL-1β (Abcam, Cat#ab214025 and Cat#ab197742) and TNF-α (Abcam, Cat#ab181421 and Cat#ab208348) Human and Mouse ELISA Kit according to the manufacturer's instructions. The lipid profile and glucose levels were measured with a Roche Cobas 6000 clinical chemistry analyzer.

Deathscreening and glycosylation gene microarray

The gene expression profiles were analyzed using human deathscreening and glycosylation PCR array according to the manufacturer's protocol (Wcgene Biotech, Shanghai, China). The data were analyzed using Wcgene Biotech software. Genes with fold-changes >2 and $p < 0.05$ were considered to be biological significant.

RNA sequencing

Total RNA was extracted by using RNAmini kit (Qiagen, Germany). mRNA enrichment, fragmentation, reverse transcription, library-construction, sequencing (Illumina NovaSeq 6000), and bioinformatic analysis were performed by Genergy Biotechnology Co., Ltd. (Shanghai, China).

Molecular docking analysis

RMSD was used to quantify the average displacement of selected atoms in a given frame relative to a reference frame. The RMSD at any time was calculated using the following equation: $\mathrm{RMSDx}=\sqrt{\frac{1}{N}\sum_{i=1}^{N}(r'_i(t_x)-r_i(t_{ref}))^2}$, where N is the number of atoms in the atom selection; t_{ref} is the reference time (typically, the first frame is used as the reference and is regarded as time t = 0); and r' is the position of the selected atoms in frame x after superimposing on the reference frame, where frame x is recorded at time t_x. The calculation was each frame in the simulation trajectory.

Rigid protein–protein docking between OGT and RIPK1 was performed using GRAMM-X (http://gramm.compbio.ku.edu/) to investigate their interaction. The protein structural domains of OGT and RIPK1 were retrieved from the Protein Data Bank (PDB) database (http://www.rcsb.org/). PyMOL (version 2.4) and PDBePISA (https://www.ebi.ac.uk/pdbe/pisa/) were used to investigate protein–protein interactions and further visual analysis, respectively.

Molecular simulation

RIPK1 and RIPK3 crystal structure was taken from Uniprot Database. The modeling structures of RIPK1 and RIPK3 were chosen from the cluster of the equilibrium period of molecular dynamics (MD) simulation, respectively. The glycosylation structure of RIPK1 at Ser331 was modeled with GlyCAM server. For the glycosylated and nonglycosylated RIPK1–RIPK3 complexes, 1 μs MD simulation was conducted in parallel with three repeats. From the cluster and PCA results of the MD trajectories, the most typical complex conformation was taken for the further study.

Generation of O-GlcNAc-specific antibody against S331 on RIPK1 (RIPK1 S331-O-GlcNAc)

The modified O-GlcNAc peptide NKS (O-GlcNAc)-Ser-EAGYS was synthesized on a Liberty microwave-assisted peptide synthesizer (CEM) using MBHA Rink amide low load resin (Novabiochem) with standard protocols of Fmoc SPS chemistry. After high performance liquid chromatograpy (HPLC) purification of the peptide, it was conjugated to keyhole limpet haemocyanin (KLH) and injected into 4 rabbits. 4 strains of antibodies from the serum were first precipitated with ammonium sulphate followed by a one-step purification by passing the resuspended antibody over a nonGlcNAcylated peptide column. The flowthrough from the column was collected and used for immunoblotting. The specificity and viability of the antibodies were verified by western blots with wild type and OGT-deficient HaCaT cells, or RIPK1- and S331-mutated-RIPK1-overexpressed HaCaT cells.

Global transcription analysis by EU

To quantify global RNA synthesis *in vitro*, we used the Click-iT RNA Alexa Fluor 488 kit (Thermo Fisher Scientific, C10329). The HaCaT cells (9,000 cells per well) were plated onto 96-well plates (Perkin Elmer, 6055300). The following day, cells were pulsed with EU for 60 minutes and then fixed with 4 % PFA/PBS for 10 minutes at room temperature. Then, the cells were permeabilized and blocked with blocking buffer (0.5% BSA, 0.1% Triton X-100 in 1×PBS) overnight at 4 ºC. The detection was performed through the Click-iT chemistry reaction for 2 h at room temperature,

following manufacturers' instructions. Finally, nuclei were counterstained with DAPI.

Dewaxing treatment

The staining rack with FFPE samples were placed into the oven at 37 °C for 30 min. Then, the staining rack was transfered into a staining jar, added heptane into the staining jar where the sample is submerged, cover the jar lid, stand at room temperature for 10 min, discard the liquid, and repeat once. Add 100 % ethanol into the staining jar to cover the sample, cover the jar lid, stand at room temperature for 5 min, and discard the liquid. Then add 90% ethanol and 75% ethanol in sequence to repeat this treatment. Adding deionized water into the dyeing jar to soak the sample; take out the samples in turn and transfer into pressure cycling technology (PCT) tubes using a clean blade to avoid contamination. Add 12.5 μL 100 mM Tris-HCl, pH 10.0 to the PCT tubes containing the samples and place them on a horizontal shaker at 95 °C with 600 rpm for 30 min.

PCT based protein digestion and desalting

30 μL 6 M Urea/2 M thiourea/100 mM triethylammonium bicarbonate (TEAB), 5 μL 200 mM tris (2-carboxyethyl) phosphine (TCEP) and 2.5 μL 800 mM iodoacetamide (IAA) was added for reduction and alkylation under 45000 psi, with 30 s high pressure and 10 s ambient pressure per cycle, 30 °C for 90 cycles. 85 μL 0.1 M TEAB was added into PCT tube. Then 10 μl Trypsin (0.5 μg/ul), 5 μl Lys−C (0.25 μg/μl) were added for protein digestion under 20000 psi, with 50 s high pressure and 10 s ambient pressure per cycle, 30 ℃ for 120 cycles. Tryptic peptides were transferred into 1.5 mL tubes and digestion was then terminated by 15 μL 10 % trifluoroacetic acid (TFA). Sample pH was adjusted to 2–3. SOLAμ (Thermo Fisher Scientific™, San Jose, USA) was applied for desalting and TMTpro 16plex Isobaric Label Reagent Set was applied for TMT labeling according to their user guide.

Enrichment of O-GlcNAcylated peptides and LC–MS/MS analysis

Human primary keratinocytes were treated with LL-37 (50 μg/ml) and Ac2-26 (50 ng/ml) for 30 h or transfected with the OGT plasmid, then lysed in 8 M urea buffer containing a protease inhibitor. The lysates were sonicated three times, and the clarified supernatants were digested with trypsin. Tryptic peptides were dissolved in

NETN buffer and incubated with prewashed antibody-bound beads (PTM Bio, PTM954) at 4 °C overnight. The beads were subsequently washed four times with NETN buffer and twice with deionized water. Bound peptides were eluted with 0.1% trifluoroacetic acid, pooled, vacuum-dried, and desalted using C18 ZipTips (Millipore).

Tryptic peptides were dissolved in solvent A (0.1% formic acid and 2% acetonitrile) and loaded onto a homemade reverse-phase analytical column (25 cm length, 100 μm i.d.). Peptides were separated on a NanoElute UHPLC system (Bruker Daltonics) using a gradient of solvent A and solvent B (0.1% formic acid in acetonitrile) at a constant flow rate of 450 nl/min: 0–40 minutes, 7–24% B; 40–52 minutes, 24–32% B; 52–56 minutes, 32–80% B; and 56–60 minutes, 80% B. Peptides were analyzed on a timsTOF Pro mass spectrometer in PASEF mode with an MS/MS scan range of 100–1700 m/z.

LC–MS/MS

LC-MS/MS with the nanoflow DIONEX UltiMate 3000 RSLCnano System coupled to an Orbitrap Exploris 480 mass spectrometer (Thermo Scientific™, San Jose, USA), which equipped with a FAIMS Pro™ (Thermo Scientific™, San Jose, USA) , in data dependent acquisition (DDA) mode. Buffer A: 2% ACN, 98% H_2O containing 0.1% FA; Buffer B: 98% ACN in water containing 0.1% FA. All reagents were MS grade For each acquisition, peptides were loaded onto a precolumn (3 μm, 100 Å, 20 mm×75 μm i.d.) at a flowrate of 6 μL/min for 4 min and then injected using a 30 min LC gradient (from 7% to 30% buffer B) at a flowrate of 300 nL/min (analytical column, 1.9 μm, 120 Å, 150 mm×75 μm i.d.). Buffer A was 2% ACN, 98% H_2O containing 0.1% FA, and buffer B was 98% ACN in water containing 0.1% FA. All reagents were MS grade. The m/z range of MS1 was 375–1800 with the resolution at 60,000, normalized AGC target of 300% with the intensity threshold of 2e4, and maximum ion injection time (max IT) of 50 ms. MS/MS experiment were performed with a resolution at 30000, normalized AGC target of 200%, and max IT of 86 ms. isolation window was set to 0.7 m/z and first mass was set to 110 m/z.

Mass spectrometry data analysis

The mass spectrometry data were processed using Fragpipe software (version 19.1), uniprot fasta files(2023-05-15-reviewed-contam-UP000005640_human_pd.fasta). Carbamidomethylation of cysteine and methionine of N-termini was set as a static modification, while oxidation of methionine was set as a variable modification. This comprehensive analysis provided both qualitative and quantitative data, applying a stringent threshold for the false discovery rate (FDR) of less than 0.01 as the filtering criterion.

Database search

MS/MS data were processed using MaxQuant software (v.1.6.15.0). Tandem mass spectra were searched against Homo_sapiens_9606_SP_20230103.fasta (20389 entries) concatenated with the reverse decoy and contaminants database. Trypsin/P was specified with up to 2 missing cleavages. The minimum peptide length was set to 7, and the maximum number of modifications per peptide was 5. The mass tolerances were 20 ppm for precursor ions (first and main search) and 20 ppm for fragment ions. Carbamidomethylation of cysteine was set as a fixed modification. The acetylation of protein N-termini, oxidation of methionine, and O-glycosylation of serine/threonine were set as variable modifications. The false discovery rate (FDR) for proteins, peptides, and peptide-spectrum matches (PSMs) was adjusted to <1%.

Non-target metabolomics analysis

Skin lesions and serum from SJS/TEN patients and mouse models, or human primary keratinocytes treated with LL-37 and Ac2-26, were used for metabolomics analysis. Cells were washed twice with LC–MS grade PBS, scraped, snap-frozen in liquid nitrogen, and stored at -80 °C. Metabolites were extracted using cold methanol/acetonitrile/water solution (2:2:1) via freeze-thaw cycles in liquid nitrogen. Extracted metabolites were resuspended in acetonitrile/H_2O (v:v,1:1) and analyzed by LC–MS/MS on a UPLC–TripleTOF 5600^+ system (SCIEX). Data processing was performed using MarkerView software (SCIEX).

Statistical and bioinformatics analysis

All the statistical and bioinformatics was performed in R (version 4.0). Missing value was imputed with seqKNN (version 1.0.1). Principal Components Analysis

(PCA) was conducted to visualize the separation of each groups using the stats package in R.

R package clusterProfiler was used to perform the Gene ontology (GO) and Kyoto Encyclopedia of Genes and Genomes (KEGG) enrichment analysis. GSEA was performed by the R/Bioconductor package clusterProfiler. The enrichment score (ES) in GSEA was calculated by first ranking the fold change of proteins from the most to least significant with respect to the two phenotypes, the entire ranked list was then used to assess how each gene set were distributed across the ranked list. Protein–Protein interactions (PPI) analysis was performed by STRING: functional protein association networks (https://string-db.org/).

SUPPLEMENTARY FIGURE LEGENDS

Fig. S1 Impaired O-GlcNAcylation signaling in patients and mouse models with SJS/TEN. (A) RT–PCR showing the *OGT* and *OGA* mRNA levels in skin lesions from TEN patients. **(B)** RT–PCR showing the *OGT* mRNA levels in an SM164-induced TEN-like mouse model. *ns*, not significant, ***$P < 0.001$; n=3 per group.

Fig. S2 Nucleolar stress signature in SJS/TEN skin lesions and cell models. (A) RPL5 and RPL11 immunostaining (*scale bar = 100 μm*). **(B)** Western blots showing the levels of RPL5 and RPL11 in skin lesions from TEN patients. **(C)** Western blots showing the levels of RPL5 and RPL11 in skin lesions and non-lesional skin from TEN patients. **(D–E)** Keratinocytes were treated with LL-37/Ac2-26. The levels of RPL (top) and RPS (bottom) were determined using RT–PCR and western blots. **(F–G)** Keratinocytes were treated with LL-37/Ac2-26. The levels of NCL and FBL were determined using RT–PCR and western blots. **(H)** Representative confocal microscopy images with NCL and DAPI and with FBL and DAPI as well as representative confocal microscopy images of FBL, NCL, and DAPI staining (nuclei were stained with DAPI) (*scale bar = 50 μm*). **(I)** Western blot showing the level of p53. *$P < 0.05$, **$P < 0.01$, ***$P < 0.001$; two-tailed t-test.

Fig. S3 HBP activity and glucose uptake are attenuated in individuals with SJS/TEN. (A) Schematic of glucose metabolism pathways highlighting HBP enzymes (red) and key metabolites. **(B)** Heatmap of differentially expressed metabolites in keratinocytes treated with LL-37/Ac2-26. n = 3 technical replicates per group. Heatmap analyses of metabolites in **(C)** serum or **(D)** skin lesions from TEN patients. **(E)** Western blots showing the levels of the key HBP enzymes in LL-37/Ac2-26-treated keratinocytes. **(F)** Western blots showing the levels of GNA1 and GLUT1 in TEN lesions or **(G)** restoration of GNA1 and GLUT1 levels in TEN lesions after corticosteroid treatment. **(H–I)** Measurement of glucose uptake (2-NBDG assay) **(H)** and GLUT1/GLUT3 levels **(I)** in LL-37/Ac2-26-treated keratinocytes. **(J)** GNA1 and GLUT1 immunostaining (*scale bar = 100 μm*). *ns*, not significant. $*P < 0.05$, $**P < 0.01$, $***P < 0.001$.

Fig. S4 HBP activity and glucose uptake are attenuated in SJS/TEN mouse models. (A) PCA analyses of differentially expressed metabolites between WT and SM164-induced TEN-like mouse model. **(B)** Volcano plot and **(C)** heatmap analyses of metabolites in serum from SM164-induced TEN-like mouse model. **(D)** Western blots showing the levels GNA1 and GLUT1 in skin lesions from SM164-induced TEN-like mouse model. **(E)** GNA1 and GLUT1 immunostaining (*scale bar = 100 μm*). $**P < 0.01$.

Fig. S5 Generation and functional characterization of OGT knockout (KO) HaCaT cells. (A) The gRNA and cutting site was chosen to be immediately downstream of the start codon for OGT so indel's introduced by nonhomologous repair of the double-stranded break would likely disrupt the protein reading frame. **(B)** DNA sequence analysis showed the presence of the OGT mutation in clones #1-10, #1-13, #1-19, and #1-23. The black arrows indicate the heterogeneous genomic DNA sequences in each cell lines. **(C)** CRISPR/Cas9 introduced the insertion and deletion (indel) mutation in the target sites. **(D)** Western blot and **(E)** RT–PCR showing the level of OGT. **(F–O)** OGT-KO cells were exposed to a combination of LL-37 and Ac2-26. **(F)** CCK-8 assay. **(G)** LDH release assay. **(H)** ATP concentration. **(I)** The intracellular ROS levels. **(J–K)** The RIPK1 and RIPK3 levels were measured using

ELISA. **(L)** The necroptosis-related protein levels were analyzed using western blots. **(M)** IL-6, **(N)** TNF-α, and **(O)** IL-1β levels were measured using ELISA. *ns*, not significant, **P* < 0.05, ***P* < 0.01, ****P* < 0.001.

Fig. S6 OGT and TMG rescue necroptosis in SJS/TEN keratinocyes. (A) Western blot and **(B)** RT–PCR showing the level of OGT after siRNA or inhibitor treatment. **(C–K)** Human primary keratinocytes were treated with LL-37 and Ac2-26, *OGT-siRNA*, OGT-inhibitor, TMG, OGT recombinant protein, or a negative control. **(C)** CCK-8 assay. **(D)** LDH release assay. **(E)** ATP concentration. **(F)** The intracellular ROS levels. **(G–H)** The RIPK1 and RIPK3 levels were measured using ELISA. **(I)** Representative TEM images showing the mitochondrial morphological changes (*scale bar = 200 nm*). **(J)** The necrosis level was determined using FACS analysis with annexin-V/PI staining. **(K)** The necroptosis-related protein levels were analyzed using western blots. The data are reported as the means ± SEMs of three independent experiments. *ns*, not significant. **P* < 0.05, ***P* < 0.01, ****P* < 0.001.

Fig. S7 OGT attenuates inflammatory response in SJS/TEN keratinocytes after *OGT* knockdown or inhibition. (A–G) Human primary keratinocytes were treated with LL-37 and Ac2-26, *OGT-siRNA* or OGT recombinant protein for 48 h. (**A)** IL-1β, **(B)** IL-6, and **(C)** TNF-α levels were measured using ELISA. The mRNA level of IL-1β **(D)**, IL-6 **(E)**, and TNF-α **(F)** were analyzed using RT–PCR. **(G)** The protein levels of NLRP3, IL-1β, IL-6 and TNF-α were analyzed using western blots. *ns*, not significant. **P* < 0.05, ***P* < 0.01, ****P* < 0.001.

Fig. S8 OGT inhibits SJS/TEN keratinocyte necroptosis and inflammatory response *in vitro.* (A–B) RT–PCR and western blot showing the level of OGT after transfection with OGT plasmid. **(C–J)** Human primary keratinocytes were treated with LL-37 and Ac2-26 or OGT plasmid for 48 h. **(C)** ATP concentration. **(D)** The intracellular ROS levels. **(E)** CCK-8 assay. **(F)** LDH release assay. **(G)** IL-1β and **(H)** IL-6 levels were measured using ELISA. **(I–J)** The cytokines and necroptosis-related protein levels were analyzed using western blots. *ns*, not significant. **P* < 0.05, ***P* < 0.01, ****P* < 0.001.

Fig. S9 OGT specifically interacts with RIPK1 and promotes RIPK1

O-GlcNAcylation. (A) RIPK1 O-GlcNAcylation in skin lesions from TEN patients and **(B)** SM164-induced TEN-like mouse model. **(C)** RIPK1 O-GlcNAcylation in HaCaT cells and OGT-KO cells. **(D)** HaCaT cells were cotransfected with RIPK1 and increasing doses of OGT; RIPK1 and OGT levels were determined using western blots. **(E)** RIPK1-transfected HaCaT cells were pretreated with DMSO or TMG, followed by cycloheximide (CHX) treatment for the indicated time points. RIPK1 stability was determined with western blotting and quantified with Image J. **(F)** Molecular dynamics analyses of ligand–receptor complexes. **(G)** Surface diagram of the OGT–RIPK1 docking model (OGT, blue; RIPK1, Green). **(H)** Interaction of amino acid residues with OGT/RIPK1 complex. **(I)** CoIP assay showing the interaction between HA-OGT and FLAG-RIPK1. **(J)** Flag-tagged RIPK1 and different concentration of HA-tagged OGT were cotransfected into HaCaT cells. The level of O-GlcNAcylation was detected using western blot. **(K)** HA-tagged OGT (WT or mutation) and Flag-labbel RIPK1 were transfected into HaCaT cells. CoIP assay with anti-Flag antibody was performed to demonstrate RIPK1 O-GlcNAcylation is dependent on the enzymatic activity of OGT. $*P < 0.05$, $**P < 0.01$, $***P < 0.001$.

Fig. S10 Overview of the proteins and peptides modified by O-GlcNAcylation. (A) PCA analyses of O-GlcNAcylated proteins. n = 3 technical replicates per group. **(B)** Subcellular localization of identified O-GlcNAcylated proteins.

Fig. S11 Combined analysis for O-GlcNAcylated and proteome proteins. (A) Venn diagram showing the general and unique proteome and O-GlcNAcylated proteins. **(B)** The number of proteins and sites were shown in bar chart between O-GlcNAcylated and proteome proteins. **(C)** Nine-quadrant scatter plot of integrated analyses of O-GlcNAcylated proteins and the global proteome. **(D)** KEGG pathway enrichment analyses of O-GlcNAcylated and proteome proteins. **(E)** Protein–protein interaction network constructed using the STRING database. Node size indicates interaction degree; left nodes represent global proteome proteins, and right nodes represent O-GlcNAcylated proteins.

Fig. S12 O-GlcNAcylation of RIPK1 at Ser331 is critical for keratinocyte necroptosis. (**A–I)** OGT KO cells were treated with LL-37/Ac2-26 and transfected

with RIPK1 or RIPK1 mutant plasmid. **(A)** CCK-8 assay. **(B)** ATP concentration. **(C)** LDH release assay. **(D)** The intracellular ROS levels. **(E)** RIPK1, **(F)** RIPK3, **(G)** IL-1β and **(H)** IL-6 levels were measured using ELISA. **(I)** The levels of necroptosis-related proteins were analyzed using western blots. **(J–K)** IP and western blot analyses of O-GlcNAcylation of RIPK1 at Ser331 under **(J)** glucose uptake inhibition or **(K)** glucose uptake conditions. *ns*, not significant. **P* < 0.05, ***P* < 0.01, ****P* < 0.001.

Fig. S13 RIPK1 O-GlcNAcylation at Ser331 modulates its interactions with CYLD and cIAP2/TRAF2. Heatmap **(A)** and volcano plot **(B)** showing the proteomic changes in RIPK1 S331A-expressing cells compared with WT-expressing cells. **(C)** Reactome pathway annotations showing the different signaling pathways. **(D)** Co-IP assay identifying interactions between RIPK1 and E3 ligases/deubiquitinases. **(E–G)** Co-IP results showing that OSMI-1 treatment **(E)** and OGT-KO **(F)** or RIPK1 S331A **(G)** enhance RIPK1–CYLD binding and reduces RIPK1–cIAP2/TRAF2 interactions. Data are representative of three independent experiments.

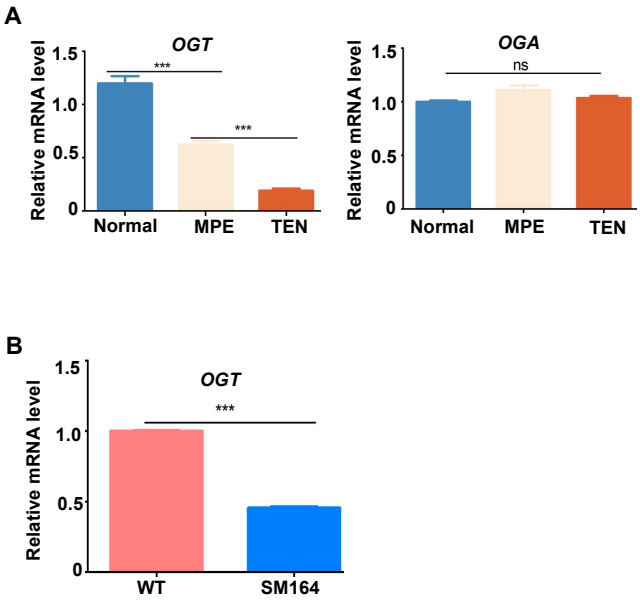
Fig. S14 O-GlcNAcylation of RIPK1 inhibits ID-mediated necroptosis and inflammatory response. (A) ATP level. **(B)** CCK-8 assay. **(C)** LDH release assay. **(D)** IL-6 and **(E)** TNF-α levels in cell supernatants after indicated treatments were measured using ELISA. Data from one of three independent experiments. **P* < 0.05, ***P* < 0.01, ****P* < 0.001.

Fig. S15 Molecular dynamics simulations reveal conformational changes induced by O-GlcNAcylation of RIPK1. (A) Initial structures of RIPK1 with the O-GlcNAcylation and mutation sites labeled and colored by atom types, respectively. **(B)** Snapshots of RIPK1–RIPK3 complexes in RIPK1 (WT), RIPK1 (Ala), and RIPK1 (O-GlcNAc) models. **(C)** The root means square deviation (RMSD) of RIPK1 and RIPK3 as a function of simulation time.

Fig. S16 O-GlcNAcase inhibition alleviates TEN severity *in vivo*. (A) Schematic of OGT and O-GlcNAcase inhibitor treatment in SMAC mimetic-induced TEN-like mouse model. **(B–I)** C57BL/6J mice were subcutaneously injected with 2 mg/kg

SM164 or vehicle (12% Captisol). Weight dependent doses of OSMI (1 mg/kg), TMG (20 mg/kg), and PugNAc (10 mg/kg) were administered intraperitoneally once daily after smac mimetic injection. Outcome assessment was performed on day 3. **(B)** Dermal thickness measurement. **(C)** Representative immunohistochemical images of RIPK1, RIPK3, and p-MLKL expression (*scale bar = 100 μm*). **(D–E)** The serum levels of IL-6 and TNF-α levels were measured using ELISA. **(F–G)** Serum levels of CK and glucose. **(H)** Immunofluorescence images of TUNEL-positive apoptotic cells (*scale bar = 100 μm*). **(I)** Representative histology of Ki67 and CD3 staining on day 3 post-SM164 injection. Insets magnify indicated area of interest (*scale bar = 100 μm*). $*P < 0.05$, $**P < 0.01$, $***P < 0.001$.

Fig. S17 The RIPK1 Ser331A-O-GlcNAc peptide exacerbates severity of TEN *in vivo*. (A–M) C57BL/6J mice were subcutaneously injected with 2 mg/kg SM164 and intravenously injected with 1 mg/kg RIPK1-O-GlcNAc peptide (started 1 day before SM164 injection). Outcome assessment was performed on day 3 (histology and clinical score). Each group contains 5 mice. **(A)** Clinical assessment. **(B)** Histology. **(C)** Lesion size. **(D)** Clinical score. **(E)** Changes in body weight. The expression of necroptosis-related proteins were analyzed using ELISA **(F–G)** and western blotting (**K**). (**H)** Spleen weight relative to body weight. (**I–J)** The serum levels of Glucose, ALT, AST, CK-MB, and LDH. (**L–M)** The serum levels of IL-6 and TNF-α were measured using ELISA. $*P < 0.05$, $**P < 0.01$, $***P < 0.001$.


A
OGT
***
***
Relative mRNA level
1.5
1.0
0.5
0
Normal
MPE
TEN
OGA
ns
Relative mRNA level
1.5
1.0
0.5
0
Normal
MPE
TEN
B
OGT
***
Relative mRNA level
1.5
1.0
0.5
0
WT
SM164

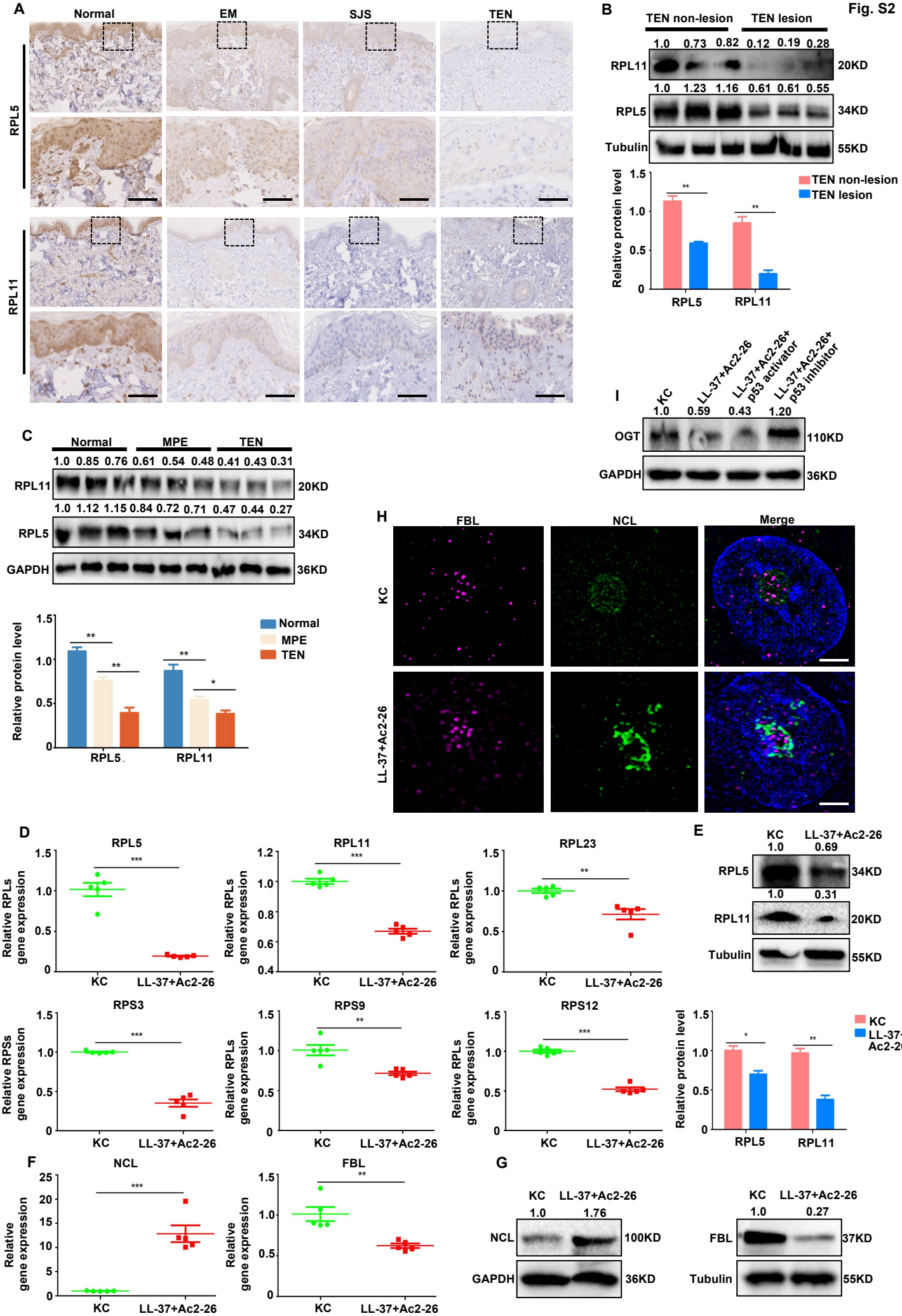
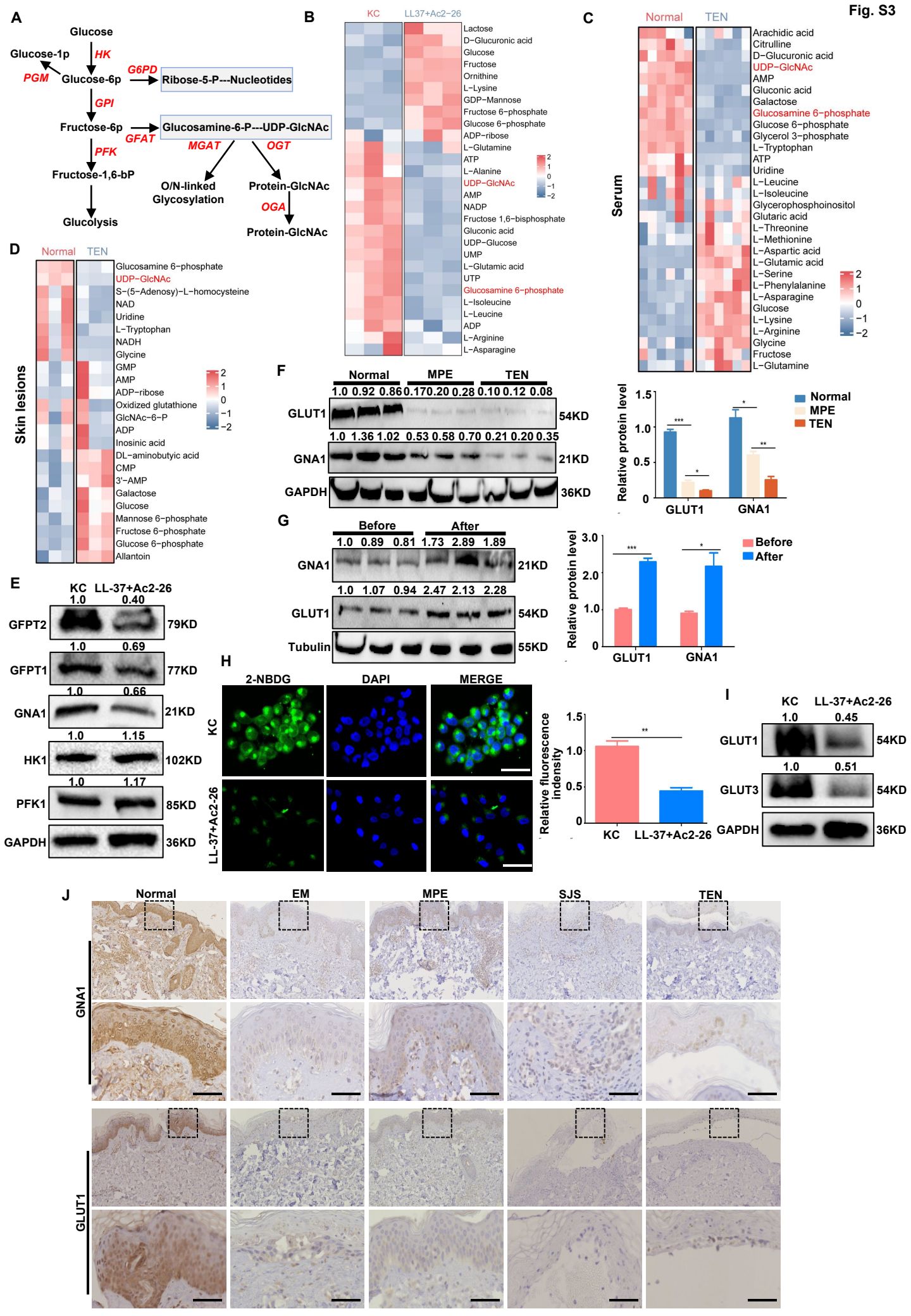

A
Normal
EM
SJS
TEN
RPL5
RPL11
B
TEN non-lesion
TEN lesion
1.0 0.73 0.82 0.12 0.19 0.28
RPL11
20KD
1.0 1.23 1.16 0.61 0.61 0.55
RPL5
34KD
Tubulin
55KD
Relative protein level
TEN non-lesion
TEN lesion
RPL5
RPL11
C
Normal
MPE
TEN
1.0 0.85 0.76 0.61 0.54 0.48 0.41 0.43 0.31
RPL11
20KD
1.0 1.12 1.15 0.84 0.72 0.71 0.47 0.44 0.27
RPL5
34KD
GAPDH
36KD
Relative protein level
Normal
MPE
TEN
RPL5
RPL11
I
KC
LL-37+Ac2-26
LL-37+Ac2-26+ p53 activator
LL-37+Ac2-26+ p53 inhibitor
1.0 0.59 0.43 1.20
OGT
110KD
GAPDH
36KD
H
FBL
NCL
Merge
KC
LL-37+Ac2-26
D
RPL5
RPL11
RPL23
RPS3
RPS9
RPS12
Relative RPLs gene expression
Relative RPSs gene expression
KC
LL-37+Ac2-26
E
KC
LL-37+Ac2-26
1.0 0.69
RPL5
34KD
1.0 0.31
RPL11
20KD
Tubulin
55KD
Relative protein level
KC
LL-37+ Ac2-26
RPL5
RPL11
F
NCL
FBL
Relative gene expression
KC
LL-37+Ac2-26
G
KC
LL-37+Ac2-26
1.0 1.76
NCL
100KD
GAPDH
36KD
1.0 0.27
FBL
37KD
Tubulin
55KD

Fig. S3


A
Glucose
Glucose-1p
HK
PGM
Glucose-6p
G6PD
Ribose-5-P---Nucleotides
GPI
Fructose-6p
GFAT
Glucosamine-6-P---UDP-GlcNAc
MGAT
OGT
PFK
Fructose-1,6-bP
O/N-linked Glycosylation
Protein-GlcNAc
OGA
Glucolysis
Protein-GlcNAc
B
KC
LL37+Ac2-26
Lactose
D-Glucuronic acid
Glucose
Fructose
Ornithine
L-Lysine
GDP-Mannose
Fructose 6-phosphate
Glucose 6-phosphate
ADP-ribose
L-Glutamine
ATP
L-Alanine
UDP-GlcNAc
AMP
NADP
Fructose 1,6-bisphosphate
Gluconic acid
UDP-Glucose
UMP
L-Glutamic acid
UTP
Glucosamine 6-phosphate
L-Isoleucine
L-Leucine
ADP
L-Arginine
L-Asparagine
C
Normal
TEN
Serum
Arachidic acid
Citrulline
D-Glucuronic acid
UDP-GlcNAc
AMP
Gluconic acid
Galactose
Glucosamine 6-phosphate
Glucose 6-phosphate
Glycerol 3-phosphate
L-Tryptophan
ATP
Uridine
L-Leucine
L-Isoleucine
Glycerophosphoinositol
Glutaric acid
L-Threonine
L-Methionine
L-Aspartic acid
L-Glutamic acid
L-Serine
L-Phenylalanine
L-Asparagine
Glucose
L-Lysine
L-Arginine
Glycine
Fructose
L-Glutamine
D
Normal
TEN
Skin lesions
Glucosamine 6-phosphate
UDP-GlcNAc
S-(5-Adenosyl)-L-homocysteine
NAD
Uridine
L-Tryptophan
NADH
Glycine
GMP
AMP
ADP-ribose
Oxidized glutathione
GlcNAc-6-P
ADP
Inosinic acid
DL-aminobutyic acid
CMP
3'-AMP
Galactose
Glucose
Mannose 6-phosphate
Fructose 6-phosphate
Glucose 6-phosphate
Allantoin
E
KC
LL-37+Ac2-26
GFPT2
1.0
0.40
79KD
GFPT1
1.0
0.69
77KD
GNA1
1.0
0.66
21KD
HK1
1.0
1.15
102KD
PFK1
1.0
1.17
85KD
GAPDH
36KD
F
Normal
MPE
TEN
1.0 0.92 0.86 0.17 0.20 0.28 0.10 0.12 0.08
GLUT1
54KD
1.0 1.36 1.02 0.53 0.58 0.70 0.21 0.20 0.35
GNA1
21KD
GAPDH
36KD
Relative protein level
Normal
MPE
TEN
GLUT1
GNA1
G
Before
After
1.0 0.89 0.81 1.73 2.89 1.89
GNA1
21KD
1.0 1.07 0.94 2.47 2.13 2.28
GLUT1
54KD
Tubulin
55KD
Relative protein level
Before
After
GLUT1
GNA1
H
2-NBDG
DAPI
MERGE
KC
LL-37+Ac2-26
Relative fluorescence indensity
KC
LL-37+Ac2-26
I
KC
LL-37+Ac2-26
GLUT1
1.0
0.45
54KD
GLUT3
1.0
0.51
54KD
GAPDH
36KD
J
Normal
EM
MPE
SJS
TEN
GNA1
GLUT1

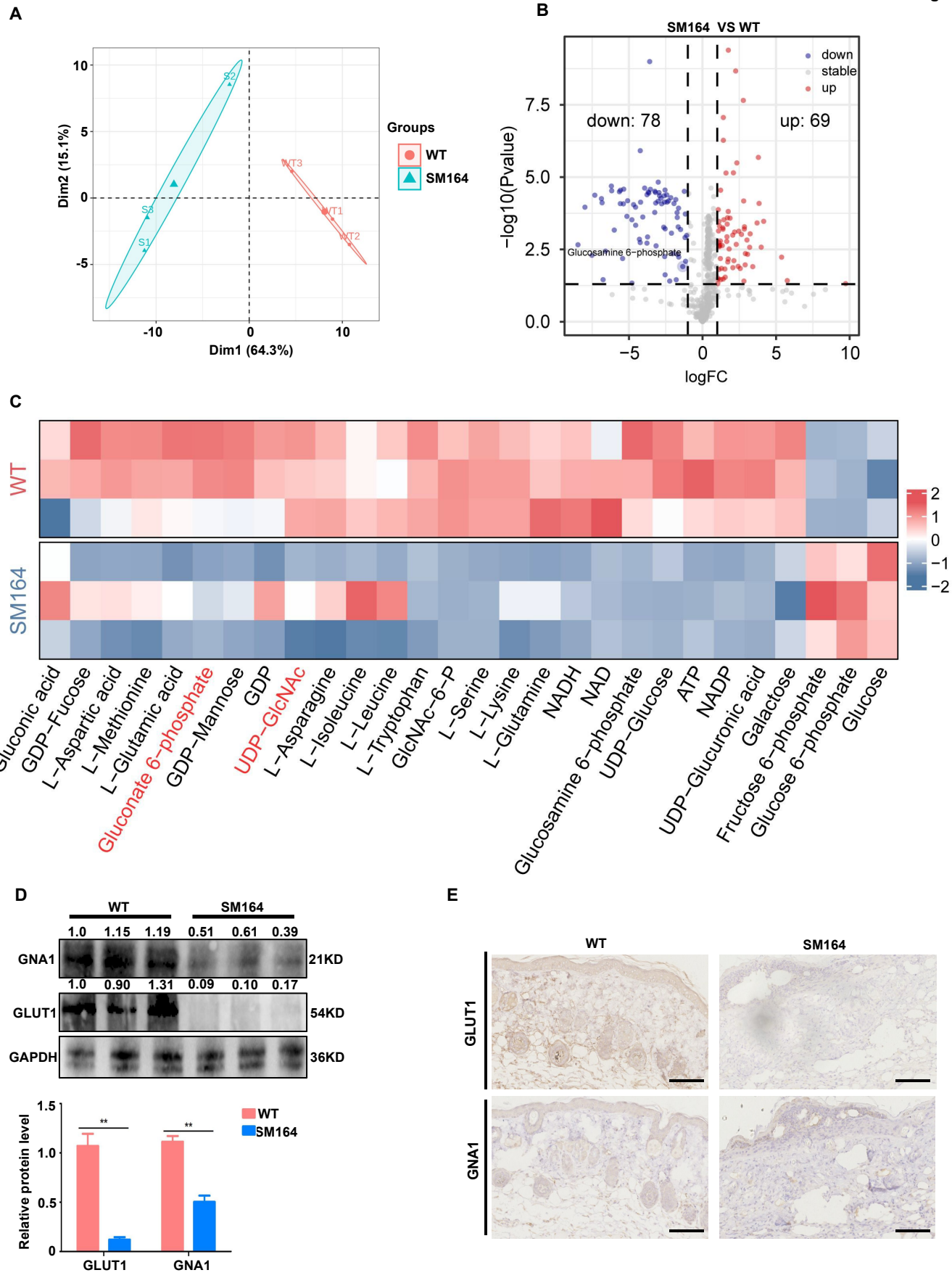

A
Dim2 (15.1%)
Dim1 (64.3%)
S1
S2
S3
WT1
WT2
WT3
Groups
WT
SM164
B
SM164 VS WT
down
stable
up
down: 78
up: 69
−log10(Pvalue)
logFC
Glucosamine 6−phosphate
C
WT
SM164
Gluconic acid
GDP−Fucose
L−Aspartic acid
L−Methionine
L−Glutamic acid
Gluconate 6−phosphate
GDP−Mannose
GDP
UDP−GlcNAc
L−Asparagine
L−Isoleucine
L−Leucine
L−Tryptophan
GlcNAc−6−P
L−Serine
L−Lysine
L−Glutamine
NADH
NAD
Glucosamine 6−phosphate
UDP−Glucose
ATP
NADP
UDP−Glucuronic acid
Galactose
Fructose 6−phosphate
Glucose 6−phosphate
Glucose
D
WT
SM164
GNA1
GLUT1
GAPDH
21KD
54KD
36KD
Relative protein level
GLUT1
GNA1
E
WT
SM164
GLUT1
GNA1

Fig. S5

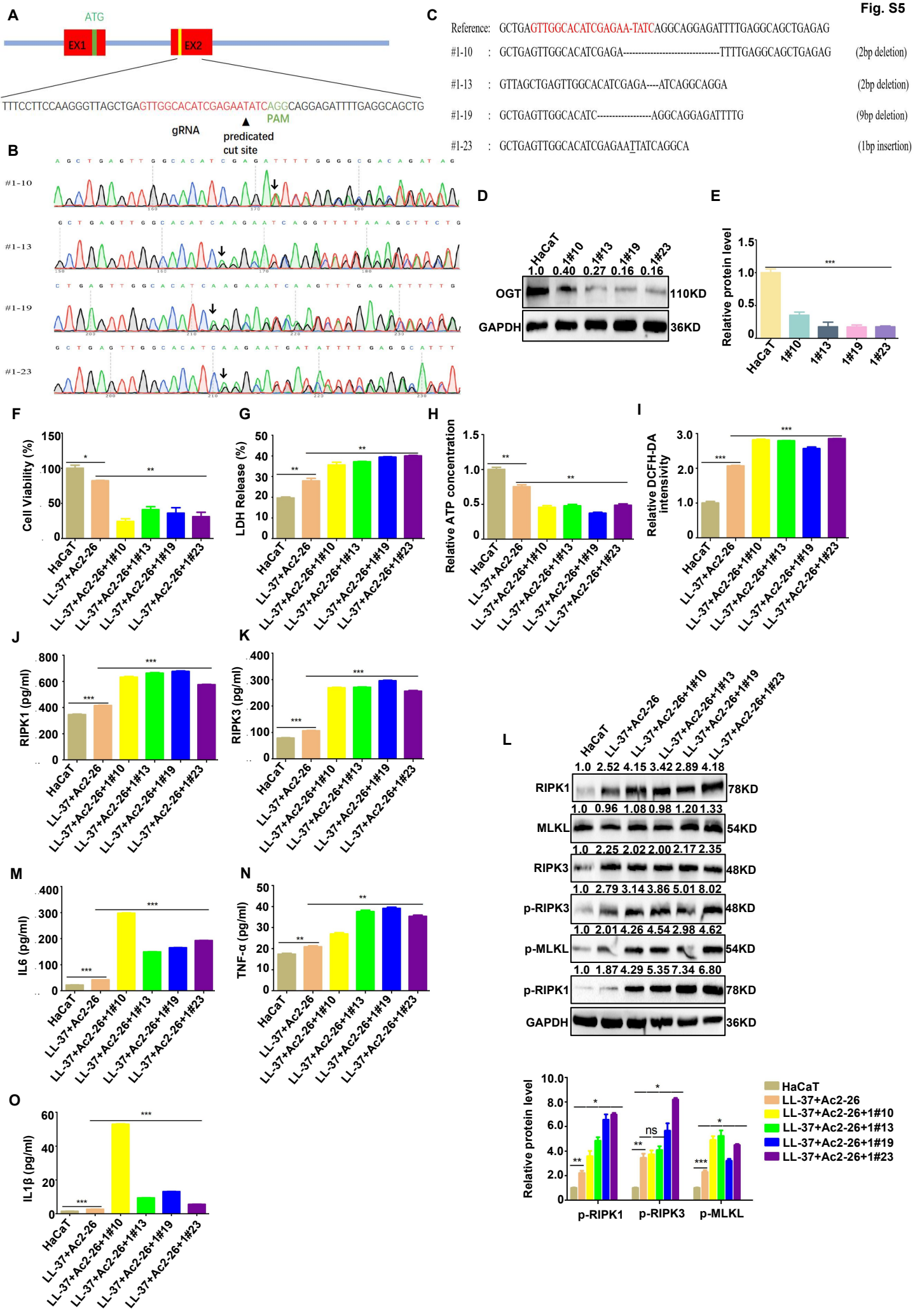
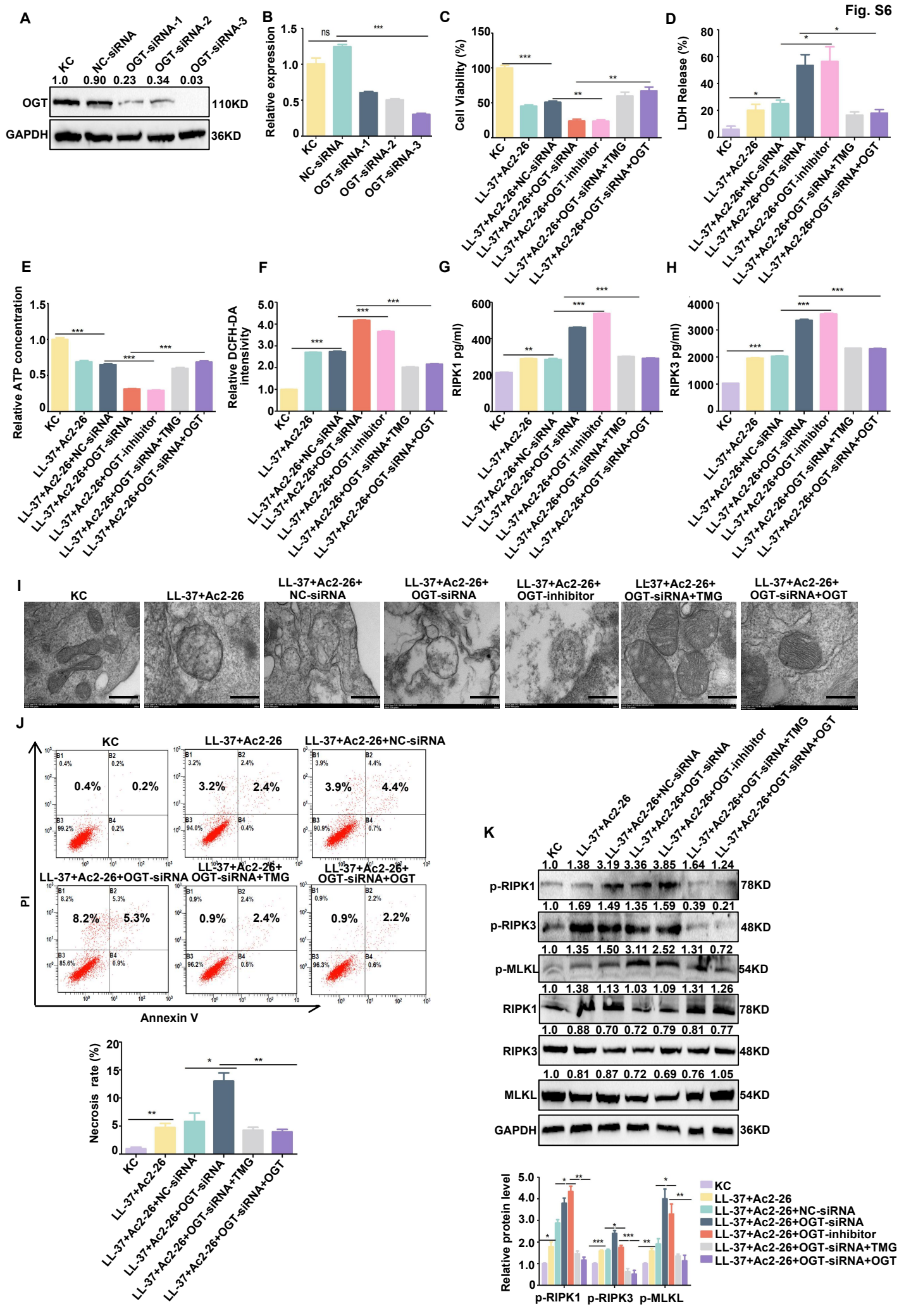
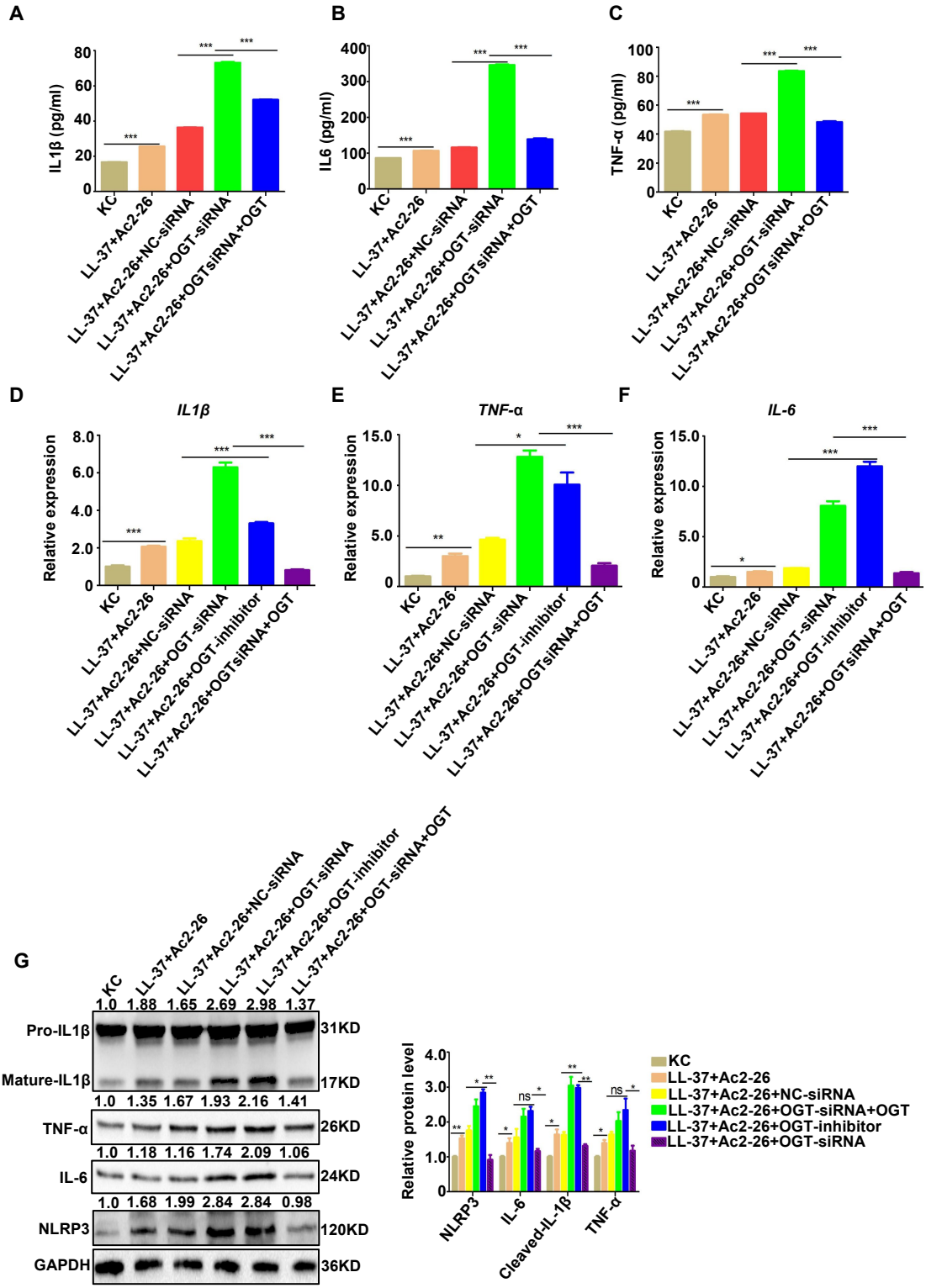
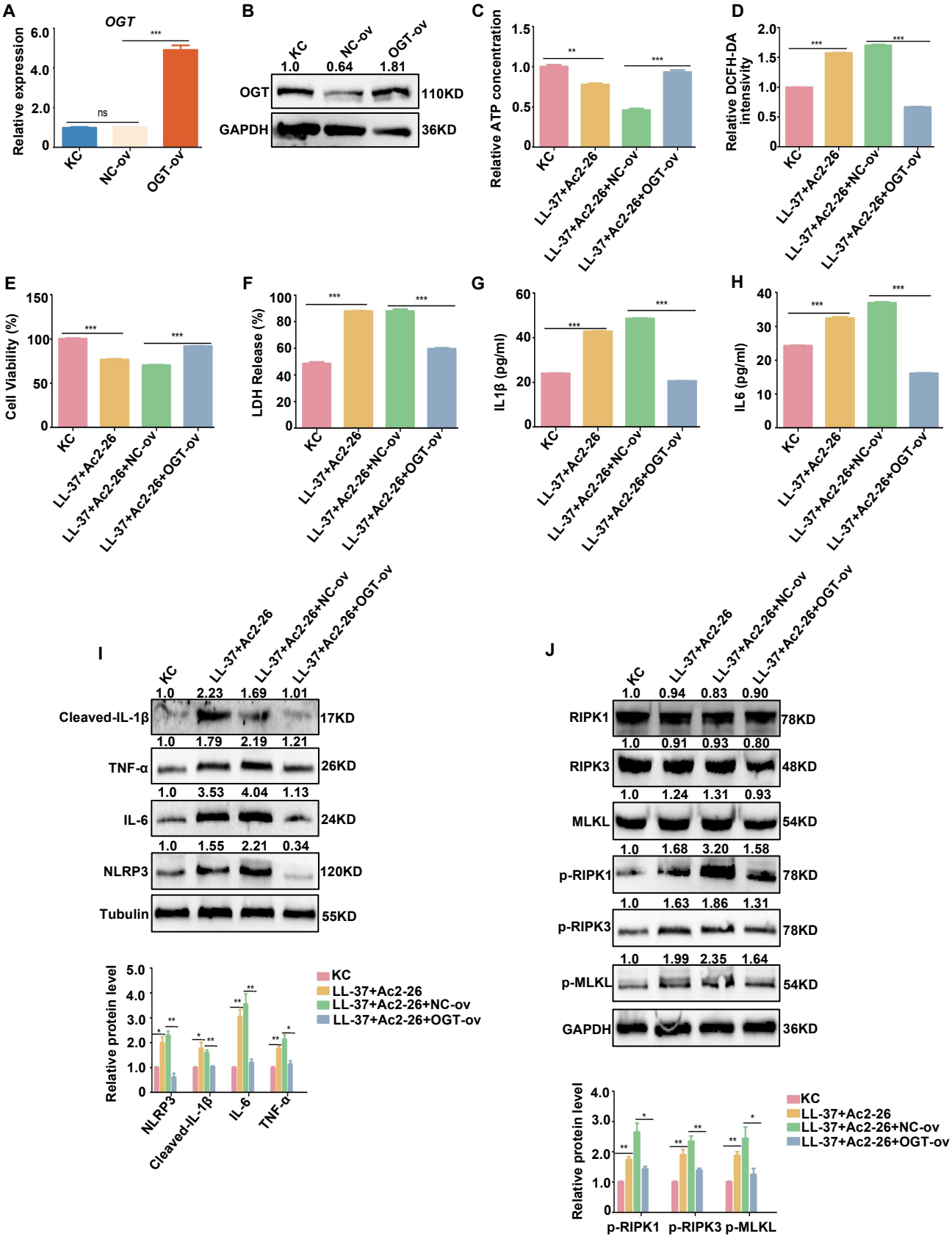
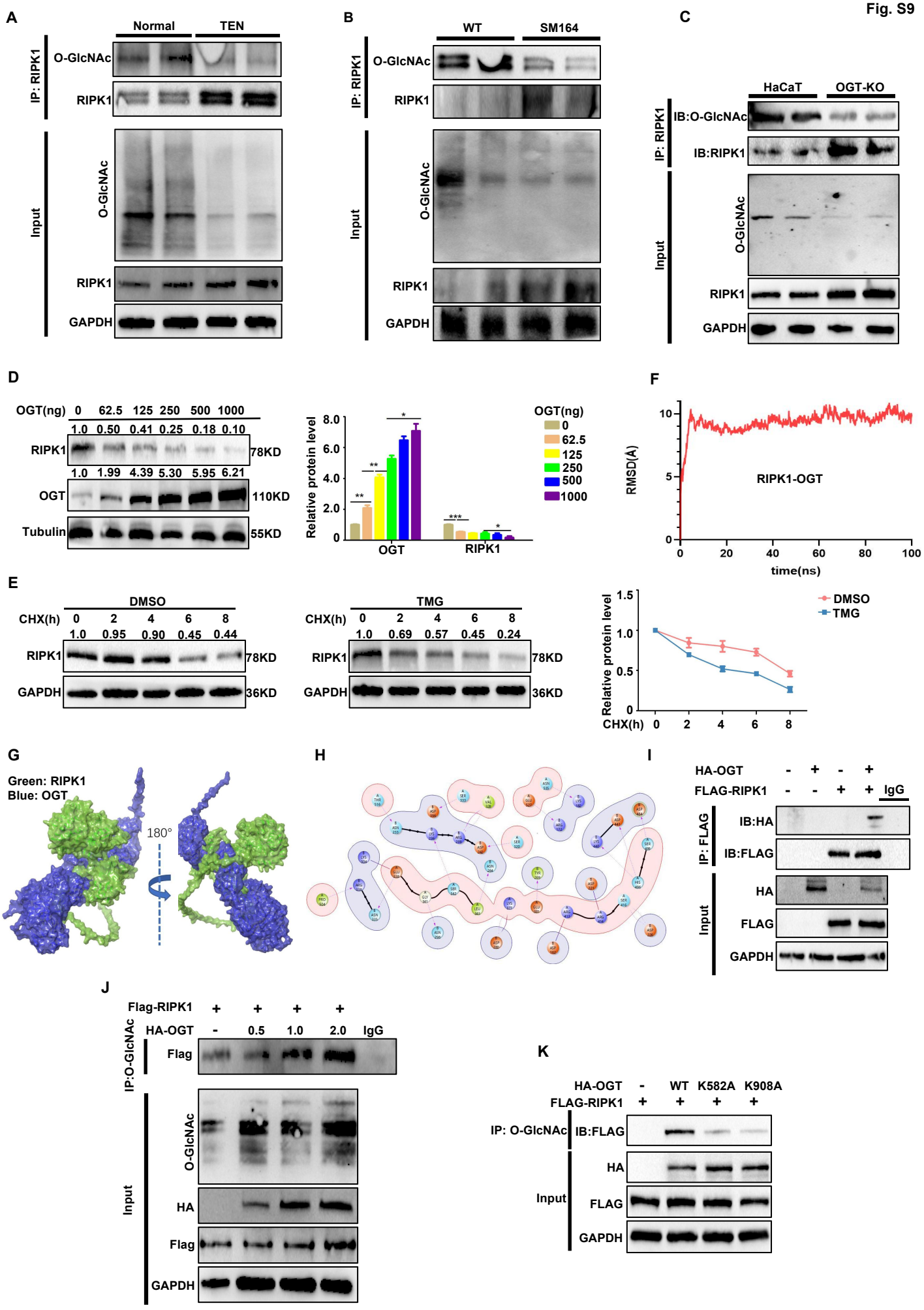

A
ATG
EX1
EX2
TTTCCTTCCAAGGGTTAGCTGAGTTGGCACATCGAGAATATCAGGCAGGAGATTTTGAGGCAGCTG
gRNA
PAM
predicated cut site
B
#1-10
#1-13
#1-19
#1-23
C
Reference: GCTGAGTTGGCACATCGAGAA-TATCAGGCAGGAGATTTTGAGGCAGCTGAGAG
#1-10 : GCTGAGTTGGCACATCGAGA----------TTTTGAGGCAGCTGAGAG (2bp deletion)
#1-13 : GTTAGCTGAGTTGGCACATCGAGA----ATCAGGCAGGA (2bp deletion)
#1-19 : GCTGAGTTGGCACATC----------AGGCAGGAGATTTTG (9bp deletion)
#1-23 : GCTGAGTTGGCACATCGAGAATTATCAGGCA (1bp insertion)
D
HaCaT 1#10 1#13 1#19 1#23
1.0 0.40 0.27 0.16 0.16
OGT 110KD
GAPDH 36KD
E
Relative protein level
HaCaT 1#10 1#13 1#19 1#23
F
Cell Viability (%)
G
LDH Release (%)
H
Relative ATP concentration
I
Relative DCFH-DA intensivity
HaCaT
LL-37+Ac2-26
LL-37+Ac2-26+1#10
LL-37+Ac2-26+1#13
LL-37+Ac2-26+1#19
LL-37+Ac2-26+1#23
J
RIPK1 (pg/ml)
K
RIPK3 (pg/ml)
L
HaCaT
LL-37+Ac2-26
LL-37+Ac2-26+1#10
LL-37+Ac2-26+1#13
LL-37+Ac2-26+1#19
LL-37+Ac2-26+1#23
1.0 2.52 4.15 3.42 2.89 4.18
RIPK1 78KD
1.0 0.96 1.08 0.98 1.20 1.33
MLKL 54KD
1.0 2.25 2.02 2.00 2.17 2.35
RIPK3 48KD
1.0 2.79 3.14 3.86 5.01 8.02
p-RIPK3 48KD
1.0 2.01 4.26 4.54 2.98 4.62
p-MLKL 54KD
1.0 1.87 4.29 5.35 7.34 6.80
p-RIPK1 78KD
GAPDH 36KD
Relative protein level
p-RIPK1
p-RIPK3
p-MLKL
ns
M
IL6 (pg/ml)
N
TNF-α (pg/ml)
O
IL1β (pg/ml)

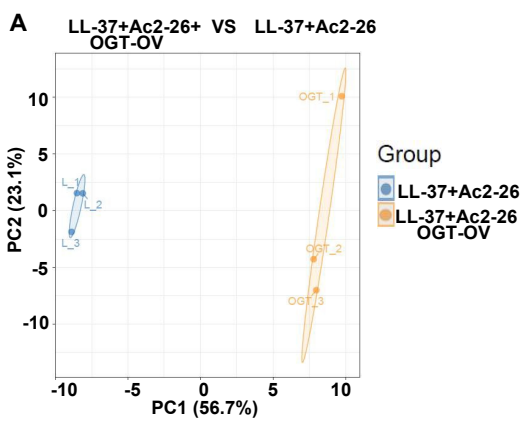
Fig. S6

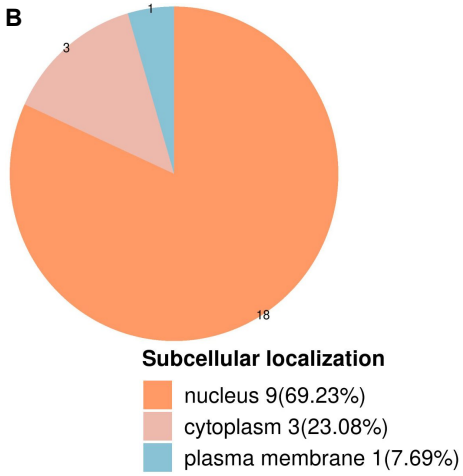

A
KC
NC-siRNA
OGT-siRNA-1
OGT-siRNA-2
OGT-siRNA-3
1.0 0.90 0.23 0.34 0.03
OGT
110KD
GAPDH
36KD
B
Relative expression
ns
***
C
Cell Viability (%)
D
LDH Release (%)
E
Relative ATP concentration
F
Relative DCFH-DA intensivity
G
RIPK1 pg/ml)
H
RIPK3 pg/ml)
KC
LL-37+Ac2-26
LL-37+Ac2-26+NC-siRNA
LL-37+Ac2-26+OGT-siRNA
LL-37+Ac2-26+OGT-inhibitor
LL-37+Ac2-26+OGT-siRNA+TMG
LL-37+Ac2-26+OGT-siRNA+OGT
I
KC
LL-37+Ac2-26
LL-37+Ac2-26+ NC-siRNA
LL-37+Ac2-26+ OGT-siRNA
LL-37+Ac2-26+ OGT-inhibitor
LL-37+Ac2-26+ OGT-siRNA+TMG
LL-37+Ac2-26+ OGT-siRNA+OGT
J
KC
LL-37+Ac2-26
LL-37+Ac2-26+NC-siRNA
LL-37+Ac2-26+OGT-siRNA
LL-37+Ac2-26+ OGT-siRNA+TMG
LL-37+Ac2-26+ OGT-siRNA+OGT
0.4%
0.2%
3.2%
2.4%
3.9%
4.4%
99.2%
94.0%
90.9%
8.2%
5.3%
0.9%
2.4%
0.9%
2.2%
85.6%
96.2%
96.3%
PI
Annexin V
Necrosis rate (%)
K
KC
LL-37+Ac2-26
LL-37+Ac2-26+NC-siRNA
LL-37+Ac2-26+OGT-siRNA
LL-37+Ac2-26+OGT-inhibitor
LL-37+Ac2-26+OGT-siRNA+TMG
LL-37+Ac2-26+OGT-siRNA+OGT
1.0 1.38 3.19 3.36 3.85 1.64 1.24
p-RIPK1
78KD
1.0 1.69 1.49 1.35 1.59 0.39 0.21
p-RIPK3
48KD
1.0 1.35 1.50 3.11 2.52 1.31 0.72
p-MLKL
54KD
1.0 1.38 1.13 1.03 1.09 1.31 1.26
RIPK1
78KD
1.0 0.88 0.70 0.72 0.79 0.81 0.77
RIPK3
48KD
1.0 0.81 0.87 0.72 0.69 0.76 1.05
MLKL
54KD
GAPDH
36KD
Relative protein level
p-RIPK1
p-RIPK3
p-MLKL
KC
LL-37+Ac2-26
LL-37+Ac2-26+NC-siRNA
LL-37+Ac2-26+OGT-siRNA
LL-37+Ac2-26+OGT-inhibitor
LL-37+Ac2-26+OGT-siRNA+TMG
LL-37+Ac2-26+OGT-siRNA+OGT

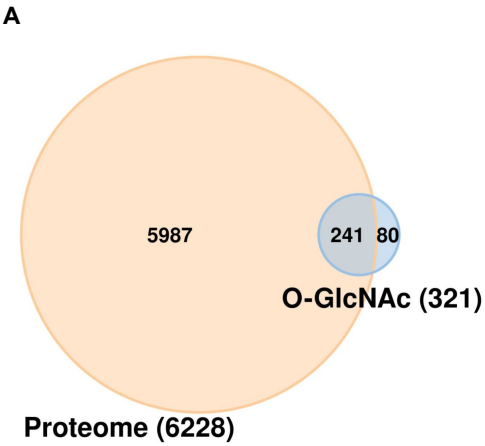

A
IL1β (pg/ml)
B
IL6 (pg/ml)
C
TNF-α (pg/ml)
KC
LL-37+Ac2-26
LL-37+Ac2-26+NC-siRNA
LL-37+Ac2-26+OGT-siRNA
LL-37+Ac2-26+OGTsiRNA+OGT
D
IL1β
E
TNF-α
F
IL-6
Relative expression
LL-37+Ac2-26+OGT-inhibitor
G
Pro-IL1β
Mature-IL1β
TNF-α
IL-6
NLRP3
GAPDH
31KD
17KD
26KD
24KD
120KD
36KD
1.0 1.88 1.65 2.69 2.98 1.37
1.0 1.35 1.67 1.93 2.16 1.41
1.0 1.18 1.16 1.74 2.09 1.06
1.0 1.68 1.99 2.84 2.84 0.98
Relative protein level
NLRP3
IL-6
Cleaved-IL-1β
TNF-α
LL-37+Ac2-26+OGT-siRNA
LL-37+Ac2-26+OGT-inhibitor
LL-37+Ac2-26+OGT-siRNA+OGT

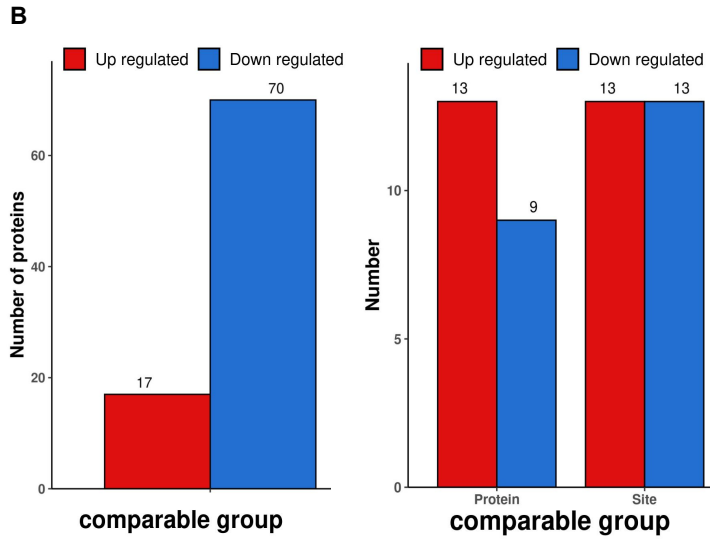

A
OGT
Relative expression
ns
***
KC
NC-ov
OGT-ov
B
KC
NC-ov
OGT-ov
1.0
0.64
1.81
OGT
110KD
GAPDH
36KD
C
Relative ATP concentration
**
***
KC
LL-37+Ac2-26
LL-37+Ac2-26+NC-ov
LL-37+Ac2-26+OGT-ov
D
Relative DCFH-DA intensivity
***
***
KC
LL-37+Ac2-26
LL-37+Ac2-26+NC-ov
LL-37+Ac2-26+OGT-ov
E
Cell Viability (%)
***
***
KC
LL-37+Ac2-26
LL-37+Ac2-26+NC-ov
LL-37+Ac2-26+OGT-ov
F
LDH Release (%)
***
***
KC
LL-37+Ac2-26
LL-37+Ac2-26+NC-ov
LL-37+Ac2-26+OGT-ov
G
IL1β (pg/ml)
***
***
KC
LL-37+Ac2-26
LL-37+Ac2-26+NC-ov
LL-37+Ac2-26+OGT-ov
H
IL6 (pg/ml)
***
***
KC
LL-37+Ac2-26
LL-37+Ac2-26+NC-ov
LL-37+Ac2-26+OGT-ov
I
KC
LL-37+Ac2-26
LL-37+Ac2-26+NC-ov
LL-37+Ac2-26+OGT-ov
1.0
2.23
1.69
1.01
Cleaved-IL-1β
17KD
1.0
1.79
2.19
1.21
TNF-α
26KD
1.0
3.53
4.04
1.13
IL-6
24KD
1.0
1.55
2.21
0.34
NLRP3
120KD
Tubulin
55KD
Relative protein level
KC
LL-37+Ac2-26
LL-37+Ac2-26+NC-ov
LL-37+Ac2-26+OGT-ov
NLRP3
Cleaved-IL-1β
IL-6
TNF-α
J
KC
LL-37+Ac2-26
LL-37+Ac2-26+NC-ov
LL-37+Ac2-26+OGT-ov
1.0
0.94
0.83
0.90
RIPK1
78KD
1.0
0.91
0.93
0.80
RIPK3
48KD
1.0
1.24
1.31
0.93
MLKL
54KD
1.0
1.68
3.20
1.58
p-RIPK1
78KD
1.0
1.63
1.86
1.31
p-RIPK3
78KD
1.0
1.99
2.35
1.64
p-MLKL
54KD
GAPDH
36KD
Relative protein level
KC
LL-37+Ac2-26
LL-37+Ac2-26+NC-ov
LL-37+Ac2-26+OGT-ov
p-RIPK1
p-RIPK3
p-MLKL

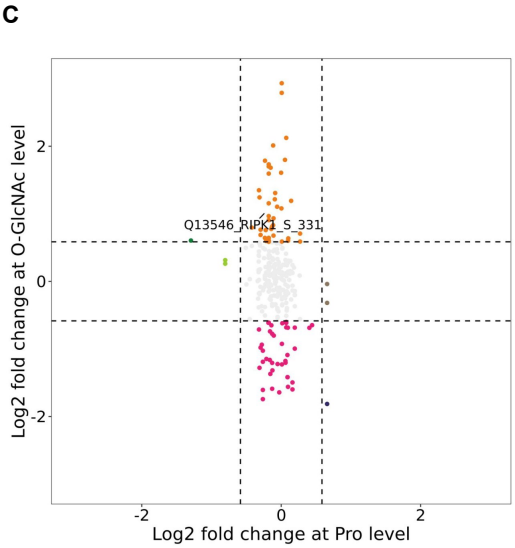

A
Normal
TEN
IP: RIPK1
O-GlcNAc
RIPK1
Input
O-GlcNAc
RIPK1
GAPDH
B
WT
SM164
IP: RIPK1
O-GlcNAc
RIPK1
Input
O-GlcNAc
RIPK1
GAPDH
C
HaCaT
OGT-KO
IP: RIPK1
IB:O-GlcNAc
IB:RIPK1
Input
O-GlcNAc
RIPK1
GAPDH
D
OGT(ng) 0 62.5 125 250 500 1000
1.0 0.50 0.41 0.25 0.18 0.10
RIPK1
78KD
1.0 1.99 4.39 5.30 5.95 6.21
OGT
110KD
Tubulin
55KD
Relative protein level
OGT(ng)
0
62.5
125
250
500
1000
OGT
RIPK1
F
RMSD(Å)
RIPK1-OGT
time(ns)
E
DMSO
CHX(h) 0 2 4 6 8
1.0 0.95 0.90 0.45 0.44
RIPK1
78KD
GAPDH
36KD
TMG
CHX(h) 0 2 4 6 8
1.0 0.69 0.57 0.45 0.24
RIPK1
78KD
GAPDH
36KD
Relative protein level
DMSO
TMG
CHX(h)
G
Green: RIPK1
Blue: OGT
180°
H
I
HA-OGT - + - +
FLAG-RIPK1 - - + + IgG
IP: FLAG
IB:HA
IB:FLAG
Input
HA
FLAG
GAPDH
J
Flag-RIPK1 + + + +
HA-OGT - 0.5 1.0 2.0 IgG
IP:O-GlcNAc
Flag
Input
O-GlcNAc
HA
Flag
GAPDH
K
HA-OGT - WT K582A K908A
FLAG-RIPK1 + + + +
IP: O-GlcNAc
IB:FLAG
Input
HA
FLAG
GAPDH

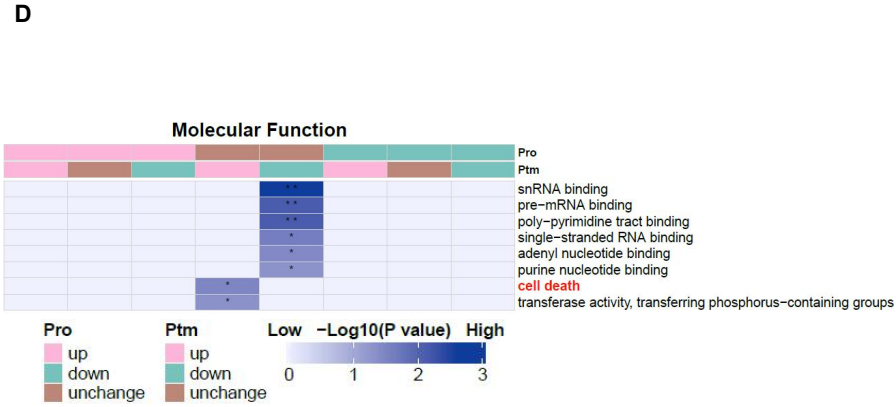

A
LL-37+Ac2-26+ VS LL-37+Ac2-26
OGT-OV
PC2 (23.1%)
PC1 (56.7%)
10
5
0
-5
-10
-10
-5
0
5
10
L_1
L_2
L_3
OGT_1
OGT_2
OGT_3
Group
LL-37+Ac2-26
LL-37+Ac2-26
OGT-OV

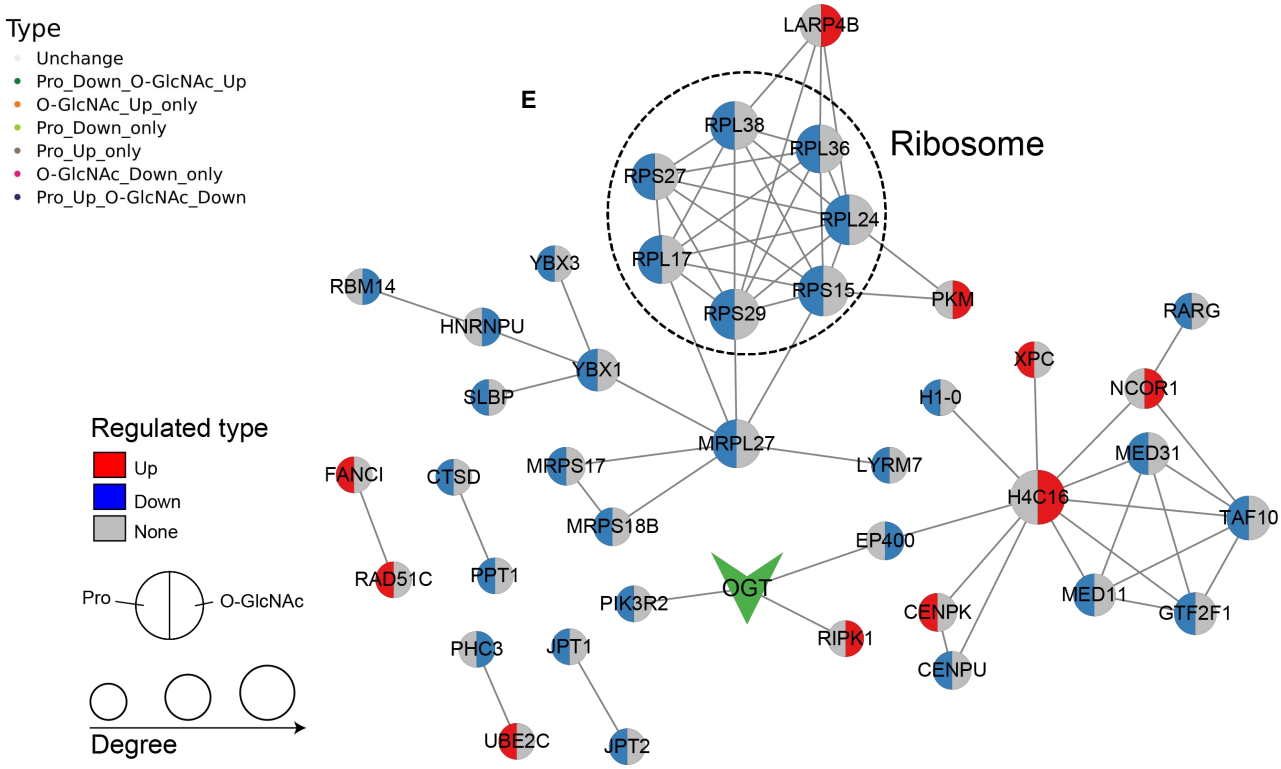

B
1
3
18
Subcellular localization
nucleus 9(69.23%)
cytoplasm 3(23.08%)
plasma membrane 1(7.69%)

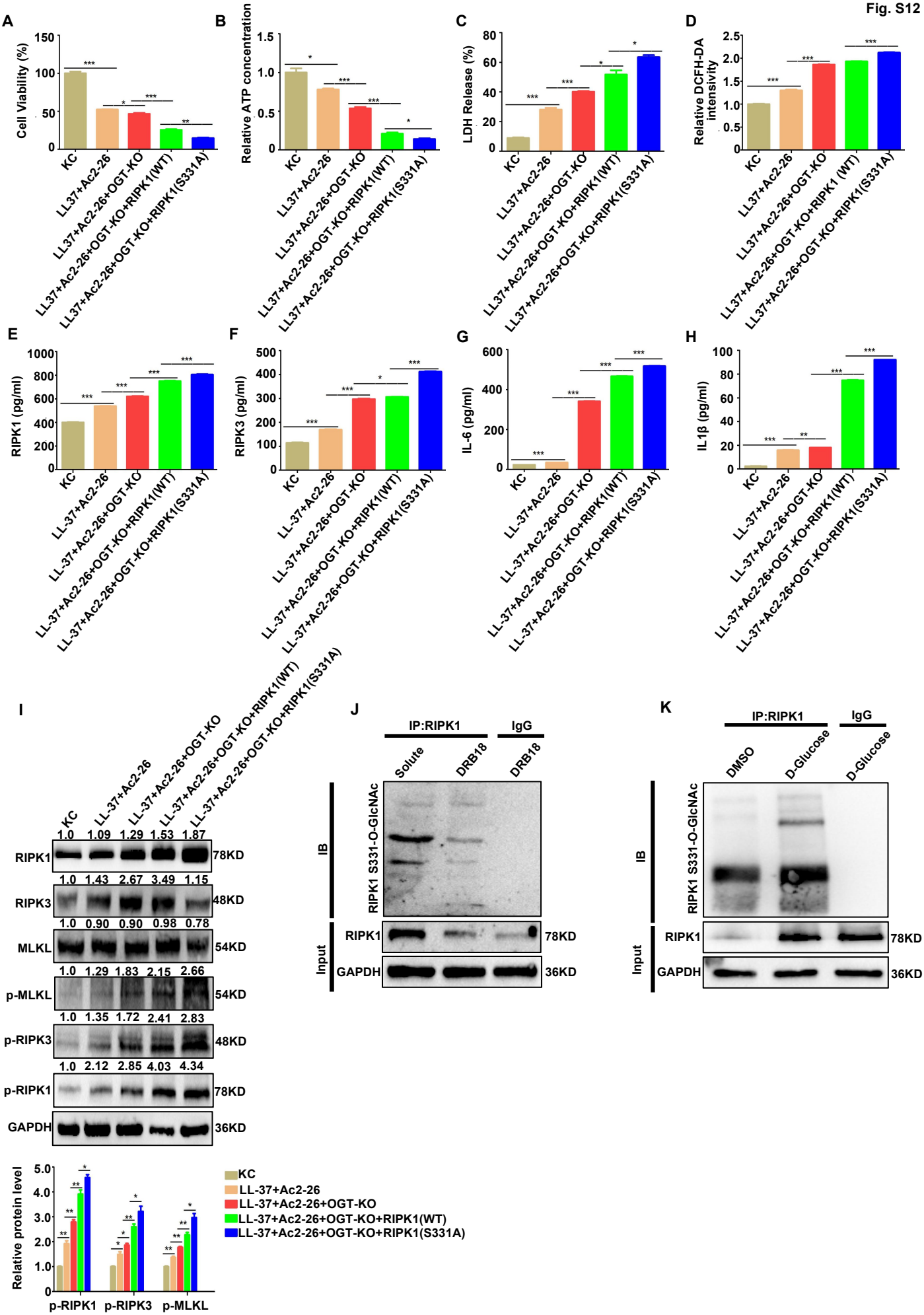

A
5987
241
80
O-GlcNAc (321)
Proteome (6228)

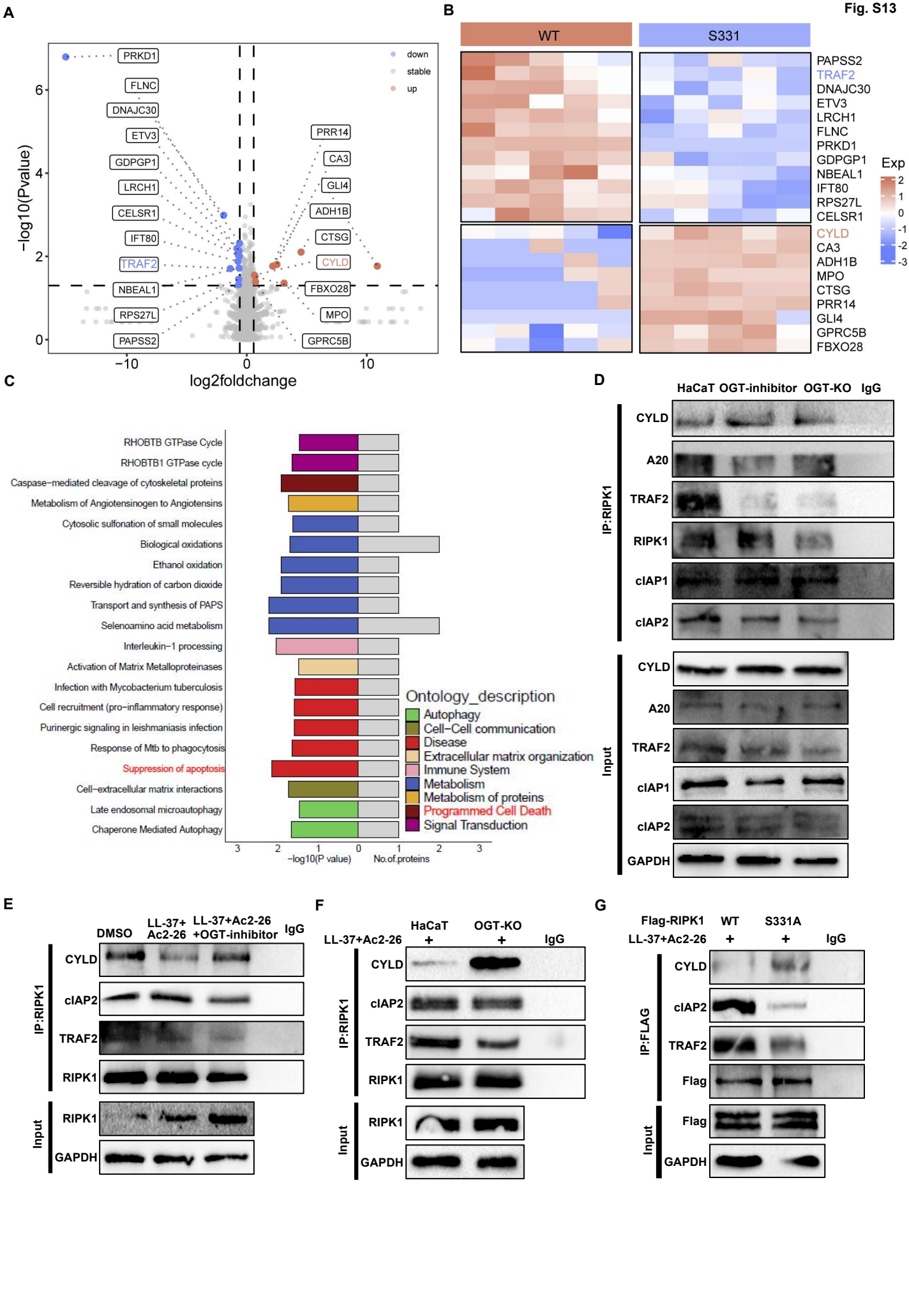

B
Up regulated
Down regulated
Number of proteins
70
17
comparable group
Number
13
9
13
13
Protein
Site
comparable group

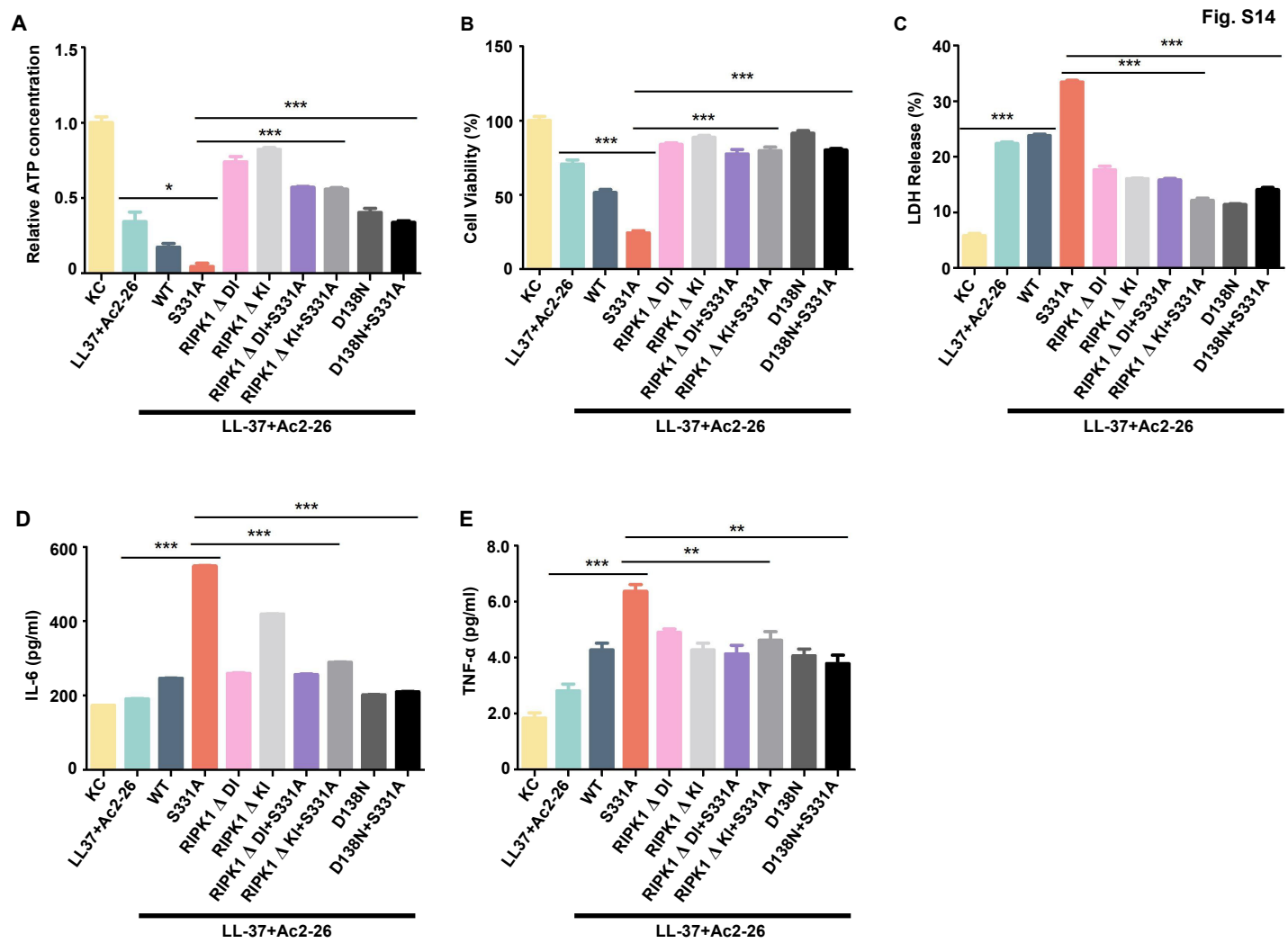

C
Log2 fold change at O-GlcNAc level
Q13546_RIPK1_S_331
Log2 fold change at Pro level

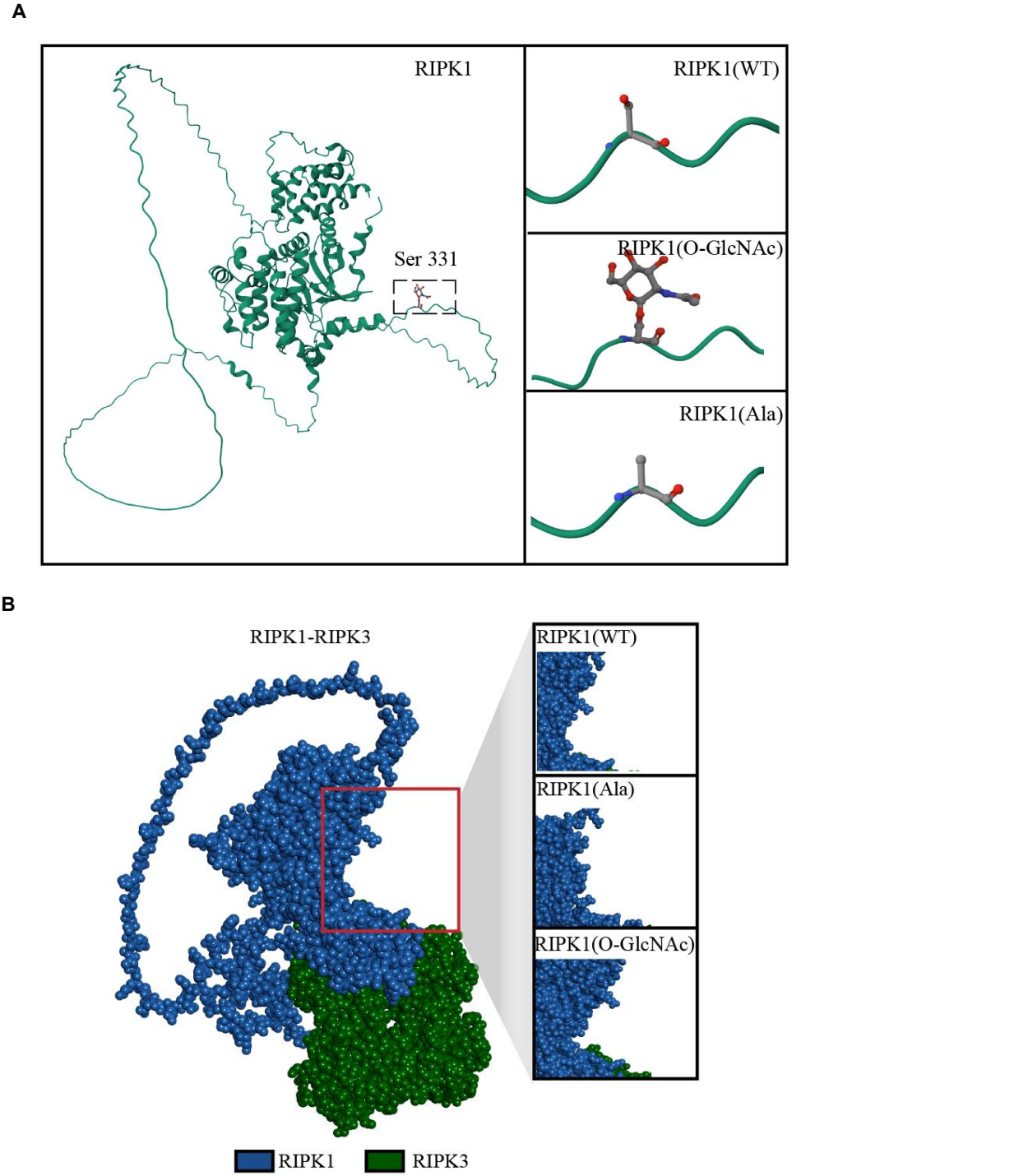

D
Molecular Function
Pro
Ptm
snRNA binding
pre−mRNA binding
poly−pyrimidine tract binding
single−stranded RNA binding
adenyl nucleotide binding
purine nucleotide binding
cell death
transferase activity, transferring phosphorus−containing groups
Pro
up
down
unchange
Ptm
up
down
unchange
Low −Log10(P value) High
0 1 2 3

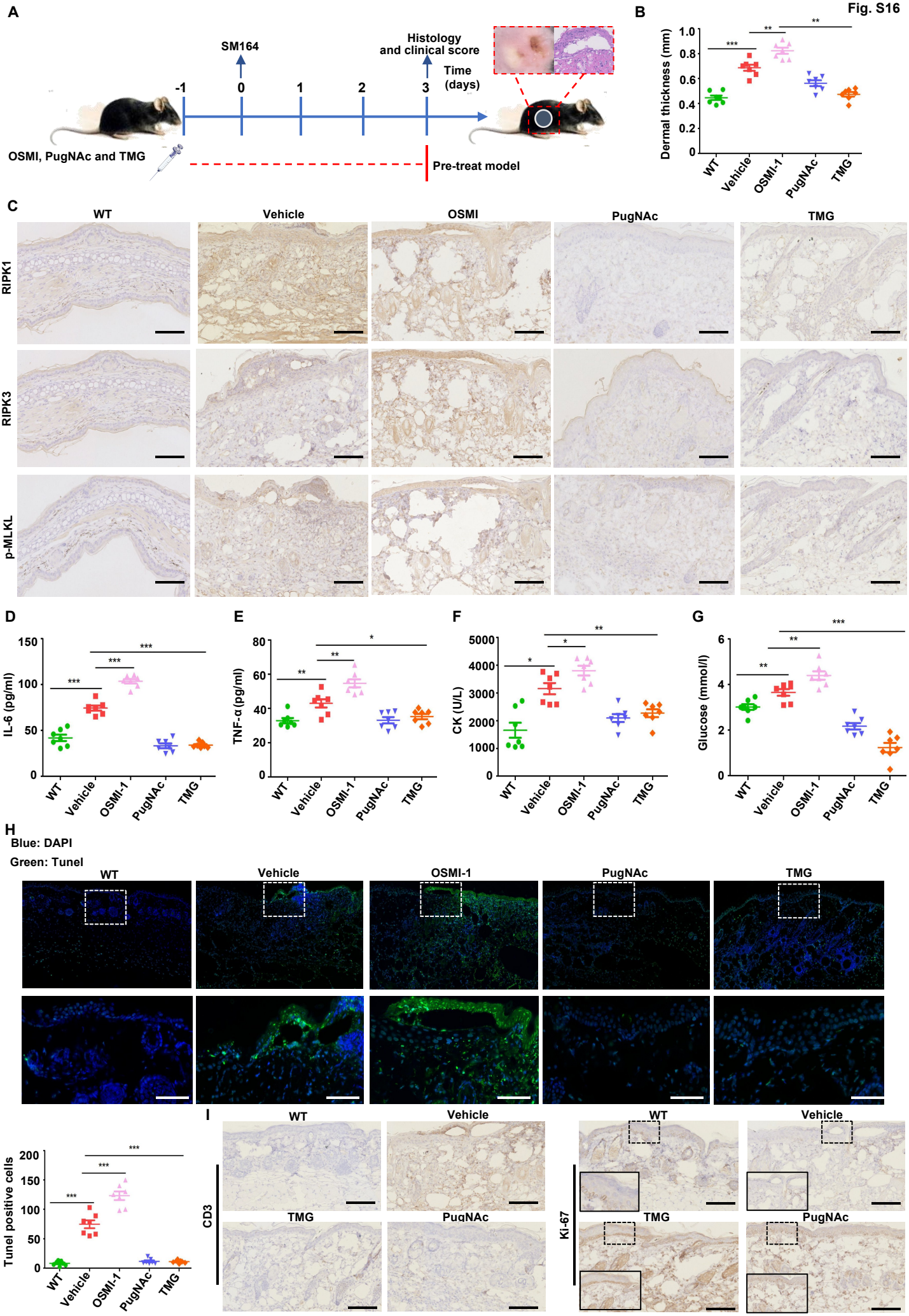

Type
Unchange
Pro_Down_O-GlcNAc_Up
O-GlcNAc_Up_only
Pro_Down_only
Pro_Up_only
O-GlcNAc_Down_only
Pro_Up_O-GlcNAc_Down
E
Ribosome
LARP4B
RPL38
RPL36
RPS27
RPL24
RPL17
RPS15
RPS29
PKM
YBX3
RBM14
HNRNPU
YBX1
SLBP
MRPL27
MRPS17
LYRM7
MRPS18B
FANCI
CTSD
RAD51C
PPT1
PHC3
JPT1
UBE2C
JPT2
PIK3R2
OGT
RIPK1
EP400
H1-0
XPC
RARG
NCOR1
MED31
H4C16
TAF10
MED11
GTF2F1
CENPK
CENPU
Regulated type
Up
Down
None
Pro
O-GlcNAc
Degree

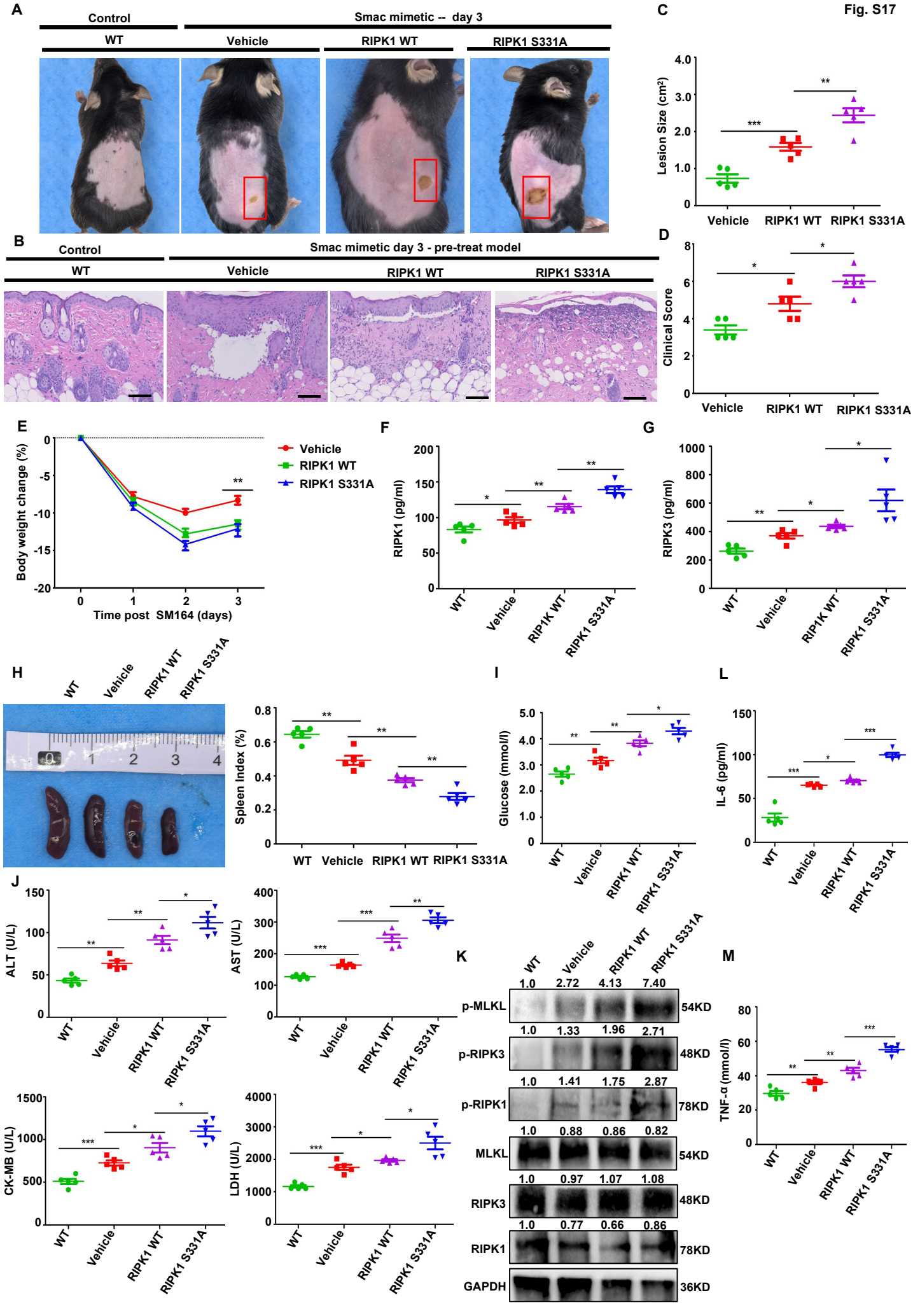

A
Cell Viability (%)
B
Relative ATP concentration
C
LDH Release (%)
D
Relative DCFH-DA intensivity
E
RIPK1 (pg/ml)
F
RIPK3 (pg/ml)
G
IL-6 (pg/ml)
H
IL1β (pg/ml)
KC
LL37+Ac2-26
LL37+Ac2-26+OGT-KO
LL37+Ac2-26+OGT-KO+RIPK1(WT)
LL37+Ac2-26+OGT-KO+RIPK1(S331A)
I
RIPK1
RIPK3
MLKL
p-MLKL
p-RIPK3
p-RIPK1
GAPDH
78KD
48KD
54KD
36KD
Relative protein level
p-RIPK1
p-RIPK3
p-MLKL
J
IP:RIPK1
IgG
Solute
DRB18
IB
RIPK1 S331-O-GlcNAc
Input
K
DMSO
D-Glucose


A
PRKD1
FLNC
DNAJC30
ETV3
GDPGP1
LRCH1
CELSR1
IFT80
TRAF2
NBEAL1
RPS27L
PAPSS2
PRR14
CA3
GLI4
ADH1B
CTSG
CYLD
FBXO28
MPO
GPRC5B
down
stable
up
−log10(Pvalue)
log2foldchange
B
WT
S331
PAPSS2
TRAF2
DNAJC30
ETV3
LRCH1
FLNC
PRKD1
GDPGP1
NBEAL1
IFT80
RPS27L
CELSR1
CYLD
CA3
ADH1B
MPO
CTSG
PRR14
GLI4
GPRC5B
FBXO28
Exp
C
RHOBTB GTPase Cycle
RHOBTB1 GTPase cycle
Caspase−mediated cleavage of cytoskeletal proteins
Metabolism of Angiotensinogen to Angiotensins
Cytosolic sulfonation of small molecules
Biological oxidations
Ethanol oxidation
Reversible hydration of carbon dioxide
Transport and synthesis of PAPS
Selenoamino acid metabolism
Interleukin−1 processing
Activation of Matrix Metalloproteinases
Infection with Mycobacterium tuberculosis
Cell recruitment (pro−inflammatory response)
Purinergic signaling in leishmaniasis infection
Response of Mtb to phagocytosis
Suppression of apoptosis
Cell−extracellular matrix interactions
Late endosomal microautophagy
Chaperone Mediated Autophagy
−log10(P value)
No.of.proteins
Ontology_description
Autophagy
Cell−Cell communication
Disease
Extracellular matrix organization
Immune System
Metabolism
Metabolism of proteins
Programmed Cell Death
Signal Transduction
D
HaCaT
OGT-inhibitor
OGT-KO
IgG
IP:RIPK1
CYLD
A20
TRAF2
RIPK1
cIAP1
cIAP2
Input
CYLD
A20
TRAF2
cIAP1
cIAP2
GAPDH
E
DMSO
LL-37+ Ac2-26
LL-37+Ac2-26 +OGT-inhibitor
IgG
IP:RIPK1
CYLD
cIAP2
TRAF2
RIPK1
Input
RIPK1
GAPDH
F
LL-37+Ac2-26
HaCaT +
OGT-KO +
IgG
IP:RIPK1
CYLD
cIAP2
TRAF2
RIPK1
Input
RIPK1
GAPDH
G
Flag-RIPK1
WT
S331A
LL-37+Ac2-26 +
+
IgG
IP:FLAG
CYLD
cIAP2
TRAF2
Flag
Input
Flag
GAPDH


A
Relative ATP concentration
1.5
1.0
0.5
0
*
***
***
KC
LL37+Ac2-26
WT
S331A
RIPK1 Δ DI
RIPK1 Δ KI
RIPK1 Δ DI+S331A
RIPK1 Δ KI+S331A
D138N
D138N+S331A
LL-37+Ac2-26
B
Cell Viability (%)
150
100
50
0
***
***
***
KC
LL37+Ac2-26
WT
S331A
RIPK1 Δ DI
RIPK1 Δ KI
RIPK1 Δ DI+S331A
RIPK1 Δ KI+S331A
D138N
D138N+S331A
LL-37+Ac2-26
C
LDH Release (%)
40
30
20
10
0
***
***
***
KC
LL37+Ac2-26
WT
S331A
RIPK1 Δ DI
RIPK1 Δ KI
RIPK1 Δ DI+S331A
RIPK1 Δ KI+S331A
D138N
D138N+S331A
LL-37+Ac2-26
D
IL-6 (pg/ml)
600
400
200
0
***
***
***
KC
LL37+Ac2-26
WT
S331A
RIPK1 Δ DI
RIPK1 Δ KI
RIPK1 Δ DI+S331A
RIPK1 Δ KI+S331A
D138N
D138N+S331A
LL-37+Ac2-26
E
TNF-α (pg/ml)
8.0
6.0
4.0
2.0
0
**
**
***
KC
LL37+Ac2-26
WT
S331A
RIPK1 Δ DI
RIPK1 Δ KI
RIPK1 Δ DI+S331A
RIPK1 Δ KI+S331A
D138N
D138N+S331A
LL-37+Ac2-26


A
RIPK1
Ser 331
RIPK1(WT)
RIPK1(O-GlcNAc)
RIPK1(Ala)
B
RIPK1-RIPK3
RIPK1(WT)
RIPK1(Ala)
RIPK1(O-GlcNAc)
RIPK1
RIPK3
C
RIPK1(WT):RIPK3
RIPK1(Ala):RIPK3
RIPK1(O-GlcNAc):RIPK3
Center of mass distance (nm)
Time (ns)
0.0
0.1
0.2
0.3
0.4
0
200
400
600


A
SM164
Histology and clinical score
Time (days)
-1
0
1
2
3
OSMI, PugNAc and TMG
Pre-treat model
B
Dermal thickness (mm)
WT
Vehicle
OSMI-1
PugNAc
TMG
C
WT
Vehicle
OSMI
PugNAc
TMG
RIPK1
RIPK3
p-MLKL
D
IL-6 (pg/ml)
E
TNF-α (pg/ml)
F
CK (U/L)
G
Glucose (mmol/l)
H
Blue: DAPI
Green: Tunel
Tunel positive cells
I
CD3
Ki-67


A
Control
WT
Smac mimetic -- day 3
Vehicle
RIPK1 WT
RIPK1 S331A
B
Control
WT
Smac mimetic day 3 - pre-treat model
Vehicle
RIPK1 WT
RIPK1 S331A
C
Lesion Size (cm²)
Vehicle
RIPK1 WT
RIPK1 S331A
D
Clinical Score
Vehicle
RIPK1 WT
RIPK1 S331A
E
Body weight change (%)
Time post SM164 (days)
Vehicle
RIPK1 WT
RIPK1 S331A
F
RIPK1 (pg/ml)
WT
Vehicle
RIP1K WT
RIPK1 S331A
G
RIPK3 (pg/ml)
WT
Vehicle
RIP1K WT
RIPK1 S331A
H
WT
Vehicle
RIPK1 WT
RIPK1 S331A
Spleen Index (%)
WT
Vehicle
RIPK1 WT
RIPK1 S331A
I
Glucose (mmol/l)
WT
Vehicle
RIPK1 WT
RIPK1 S331A
L
IL-6 (pg/ml)
WT
Vehicle
RIPK1 WT
RIPK1 S331A
J
ALT (U/L)
AST (U/L)
CK-MB (U/L)
LDH (U/L)
WT
Vehicle
RIPK1 WT
RIPK1 S331A
K
WT
Vehicle
RIPK1 WT
RIPK1 S331A
p-MLKL
1.0
2.72
4.13
7.40
54KD
p-RIPK3
1.0
1.33
1.96
2.71
48KD
p-RIPK1
1.0
1.41
1.75
2.87
78KD
MLKL
1.0
0.88
0.86
0.82
54KD
RIPK3
1.0
0.97
1.07
1.08
48KD
RIPK1
1.0
0.77
0.66
0.86
78KD
GAPDH
36KD
M
TNF-α (mmol/l)
WT
Vehicle
RIPK1 WT
RIPK1 S331A